RAFAEL RODRIGUES CARDOSO

ANÁLISE DO SPECKLE LASER DINÂMICO:
UMA RELEITURA

LAVRAS - MG
2011

RAFAEL RODRIGUES CARDOSO

ANÁLISE DO *SPECKLE LASER* DINÂMICO: UMA RELEITURA

Dissertação apresentada a Universidade Federal de Lavras, como parte das exigências do Programa de Pós-Graduação em Engenharia Agrícola, para a obtenção do título de Mestre.

Orientador

Dr. Roberto Alves Braga Junior

LAVRAS - MG
2011

Ficha Catalográfica Preparada pela Divisão de Processos Técnicos da Biblioteca da UFLA

Cardoso, Rafael Rodrigues.
Análise do speckle laser dinâmico : uma releitura / Rafael Rodrigues Cardoso. – Lavras : UFLA, 2011.
130 p. : il.

Dissertação (mestrado) – Universidade Federal de Lavras, 2011.
Orientador: Roberto Alves Braga Junior.
Bibliografia.

1. Análise de imagens. 2. Análise espectral. 3. Biospeckle laser. 4. Processamento de sinais. I. Universidade Federal de Lavras. II. Título.

CDD – 621.366

RAFAEL RODRIGUES CARDOSO

ANÁLISE DO *SPECKLE LASER* DINÂMICO: UMA RELEITURA

Dissertação apresentada a Universidade Federal de Lavras, como parte das exigências do Programa de Pós-Graduação em Engenharia Agrícola para a obtenção do título de Mestre.

APROVADA, em 10 de setembro de 2011

Dr. Roberto Alves Braga Júnior	DEG-UFLA
Dra. Thelma Sáfadi	DEX-UFLA
Dr. Giovanni Francisco Rabello	DEG-UFLA

Dr. Roberto Alves Braga Júnior

Orientador

LAVRAS - MG
2011

AGRADECIMENTOS

Agradeço a Deus, Ele tem me dado uma vida muito feliz.

Inclusive agradeço a Ele:

Pela Universidade Federal de Lavras (UFLA), ao departamento de engenharia (DEG) que abrigaram a realização desse trabalho.

Pelo Conselho Nacional de Desenvolvimento Científico e Tecnológico (CNPq) pela concessão da bolsa de estudos.

Pelo CTBE (Laboratório Nacional de Ciência e Tecnologia do Bio-etanol), que me deu uma boa oportunidade.

Por meu orientador Roberto Braga que por sua incrível (incrível mesmo!) disponibilidade e dedicação possibilitou o meu avanço para uma nova etapa.

Pelos professores Giovanni Rabelo e Thelma Sáfadi por contribuírem grandemente para a melhoria desse trabalho.

Pelos amigos e colegas do CEDIA, pelos bons momentos de trabalho e alegria que passamos juntos.

Pela minha louca família, pais, irmão (mala), primos/primas e outros loucos adotados.

Pelos demais amigos, que me ajudaram, alegraram e compartilharam comigo grandes momentos.

Por último, pela minha esposa Jovita, que tem suportado os meus descarregamentos de stress e sido a causadora da melhor fase de minha vida.

Por esses e outros motivos, obrigado Deus.

“Stay hungry; stay foolish.”

Parafraseado por Steve Jobs

RESUMO

A análise de imagem por si mesma se apresenta como um poderoso instrumento aplicado ao monitoramento a toda espécie de fenômenos biológicos. O desenvolvimento de diversos tipos de abordagens ópticas com o objetivo de se obter viabilidade na aquisição e análise de imagens tem sido um dos principais esforços nessa área de aplicação. Uma consequência desse esforço é a adoção da técnica do *biospeckle laser* como uma alternativa em potencial para se alcançar uma metrologia óptica. O *biospeckle* ou *speckle laser* dinâmico é um fenômeno formado quando um processo dinâmico ocorre em um material que é iluminado pelo *laser*. Esse fenômeno contém informações a respeito da atividade presente nesse material, seja biológico ou não. Por ser uma técnica não invasiva, não destrutiva e de custo baixo, o *biospeckle laser* (BSL) tem sido uma boa ferramenta no monitoramento de propriedades biológicas. Nesse sentido, a aplicação em instrumentação óptica tem crescido ao longo dos anos, especialmente nas áreas da biologia, medicina e agricultura. A análise do *speckle* dinâmico é feita usando técnicas de processamento digital de imagem e análises estatísticas. Contudo, essa análise tem sido um desafio para os especialistas da área devido à complexidade envolvida na interação da luz *laser* e o material em estudo. Assim, é necessário desenvolver e aperfeiçoar métodos e protocolos que assegurem maior eficiência em medir e monitorar o processo dinâmico no material em estudo. A alta sensibilidade do BSL e a variabilidade de materiais biológicos associados com o grande número de variáveis envolvidas na formação do padrão de *speckle* têm trazido grandes desafios na busca por técnicas de análise mais seguras e robustas. Esse estudo tem como objetivo desenvolver e refinar metodologias de análise do BSL e criar protocolos para diferentes tipos de análises. Em específico, são apresentados: um protocolo para separar diferentes tecidos em um mesmo material através da assinatura espectral de cada tecido e por meio da associação de resultados gráficos e numéricos do BSL; um procedimento para avaliar a qualidade de imagem durante a fase de iluminação, baseando-se na saturação, áreas escuras, formação do padrão de *speckle* e na homogeneidade da imagem; melhorias e novas abordagens na técnica do Momento de Inércia, através de uma nova normalização da matriz de ocorrência e usando quantificação contínua por meio da redução da informação temporal; e, uma nova técnica gráfica baseado no desvio padrão de cada *pixel* em relação ao tempo. Os resultados mostram a viabilidade das metodologias descritas que alcançaram maior confiabilidade e coerência na análise do BSL.

Palavras-chave: *Speckle* dinâmico. Novas técnicas de análise.

ABSTRACT

The image analysis presents itself as a powerful instrument applied to all sort of biological phenomena monitoring. The development of many optical approaches to carry out a feasible image assembling and analysis to different demands has been the main effort in this application area. A consequence of that effort is the adoption of the biospeckle laser technique as a potential alternative to pursue the optical metrology. Biospeckle or dynamic laser speckle is a phenomenon developed when a dynamic process occurs in a material under laser illumination. This phenomenon contains considerable information related to both biological and non-biological activity of the material under study. As a non-invasive, non-destructive and low cost technique, biospeckle laser (BSL) has been an outstanding tool for monitoring biological properties. Thus, its application in optical instrumentation has grown over the years, especially in the areas of biology, medicine and agriculture. Analysis of dynamic speckle laser is performed with techniques of digital image processing and statistical analysis. However this analysis has been a challenge for specialists in the area due to the complex interaction between light and material. Thus, it is necessary to develop and improve methods and protocols that ensure greater efficiency in measuring and monitoring dynamic processes in the material under study. High sensitivity of biospeckle laser (BSL) technique and variability of biological material combined with the large number of variables involved in speckle pattern formation have brought great challenges to the search for safer, more robust analysis techniques. This study aims to develop and refine methodologies for BSL analysis and create protocols for different types of analysis. In particular, it is presented: a protocol to separate different tissues in the same material by means of the frequency signature of each tissue and by means of the association of graphical and numerical results from the biospeckle laser images; a procedure to evaluate image quality during illumination, based on saturation, dark areas, speckle pattern formation and homogeneity from acquired images; improvements and new approaches in the Inertia Moment technique by means of a new occurrence matrix normalization and with continuous activity quantification reducing temporal information; and, a new graphical method based on standard deviation for each pixel in time. The results showed feasibility for methodologies described which assured more reliability and coherence for BSL analysis.

Keywords: Dynamic speckle. New analysis techniques.

SUMÁRIO

1 INTRODUÇÃO

O *speckle laser* dinâmico ou *biospeckle laser* (BSL) é um fenômeno ótico que se forma quando um material onde se desenvolve um processo dinâmico é iluminado por uma luz altamente coerente, como é o caso do *laser*. A atividade presente em materiais biológicos iluminados com o *laser*, como o crescimento e divisão celular, reações bioquímicas e movimento citoplasmático além das atividades relacionadas à água alteram as estruturas microscópicas do material. Isso faz com que a figura de interferência formada pelo espalhamento da luz no objeto varie ao longo do tempo, dando origem ao *speckle laser* dinâmico.

Essa técnica tem sido de grande destaque na avaliação e monitoramento de propriedades biológicas, por ser uma técnica não invasiva, não destrutiva e de baixo custo. Nesse sentido, vem adquirindo ao longo dos anos, uma aplicação cada vez maior na instrumentação óptica, principalmente, nas áreas de biologia, medicina e agricultura.

A análise do *speckle laser* dinâmico é feita por meio de técnicas de processamento digital de imagens e tratamento estatístico. Essas análises podem ser divididas em dois tipos básicos: as gráficas em que os resultados são mapas em que se observa a variabilidade espacial do nível de atividade no BSL, ou numérica, onde o resultado é a quantificação da atividade biológica ou não biológica no material iluminado. Além disso, as análises gráficas e numéricas podem ser feitas no domínio do tempo ou no domínio da frequência. A análise espectral do BSL apresenta algumas vantagens em muitas aplicações, pois, com a filtragem de frequências pode-se obter melhores resultados na identificação e interpretação de fenômenos que ocorrem no material em estudo, possibilitando a busca por marcação em frequência.

A análise do BSL, principalmente em materiais biológicos, tem sido um

desafio para especialistas da área, devido à complexidade envolvida na interação entre a luz e o material em análise. A alta sensibilidade da técnica do BSL e a variabilidade do material biológico associada ao grande número de variáveis envolvidas na formação do padrão do *speckle* têm causado grandes desafios para a busca de técnicas de análise mais seguras e robustas. Este trabalho visa desenvolver e aperfeiçoar técnicas de análise do BSL no sentido de garantir uma maior precisão e coerência nos resultados.

De forma especifica:

a) isolar fenômenos no BSL por meio da geração de mapas espectrais;
b) apresentar um protocolo para a associação de análise numérica e gráfica por meio da homogeneidade no BSL;
c) proposta de um pré-processamento para avaliar a qualidade da imagem resultante da iluminação, relacionada com o nível de saturação e áreas escuras nas imagens, homogeneidade da imagem e nível de formação do padrão de *speckle*;
d) apresentar alternativa à técnica do MI, usando nova normalização;
e) desenvolver uma técnica numérica de quantificação contínua;
f) desenvolver uma nova técnica gráfica com menor exigência de máquina.

2 REFERENCIAL TEORICO

2.1 Instrumentação óptica

A instrumentação é um campo multidisciplinar, envolvendo diversas áreas da ciência. O trabalho com desenvolvimento de instrumentos de controle e medição com base em princípios ópticos requer conhecimentos da física clássica e moderna, estatística e engenharia. A combinação de sistemas de aquisição e processamento digital de imagens constitui uma ferramenta importante para os pesquisadores desenvolverem novas técnicas para avaliação da qualidade de produtos vegetais de forma não destrutiva. Técnicas recentes, que utilizam uma fonte *laser* e um sistema de aquisição e processamento de imagens, têm sido referidos na literatura como visão artificial ou "*machine vision*" e ainda como "*laser vision*" (RABELO et al., 2000). Uma grande vantagem de técnicas ópticas está na sua robustez e versatilidade além de serem métodos de análise não destrutivos (TCHVIALEVA et al., 2010).

2.2 O *Laser* – considerações gerais

A luz gerada por meio de emissão estimulada tem por consequência propriedades singulares, tais como, a sua alta coerência e a sua quase-monocromaticidade e no caso do *laser*, ainda apresenta alta direcionalidade muito usada na indústria para alinhamentos e corte. Essas características têm sido aproveitadas em diversos campos da ciência e em inúmeras aplicações.

O campo aqui abordado refere-se ao uso do *laser* como fonte de iluminação em sensores ópticos capazes de detectar atividades biológicas, como é o trabalho com viabilidade de sementes apresentado por Braga et al. (2003) ou mesmo em atividades não biológicas, como sensor que mede a velocidade de

secagem (FACCIA et al., 2009).

São vários os tipos de *lasers* disponíveis, mas, normalmente, as características de interesse que os diferenciam são: a potência, o comprimento de onda bem definido, o diâmetro do raio, a divergência e, principalmente, a coerência. As características especiais do *laser* têm despertado os pesquisadores para a potencialidade de sua aplicação em investigações cientificas e na indústria. A elevada intensidade e a grande direcionalidade do feixe de um *laser* o torna interessante para um grande número de aplicações, todavia é a coerência que permite a observação e a utilização do fenômeno do *speckle* como base para o monitoramento da dinâmica de processos presentes nos objetos iluminados.

2.3 *Speckle*

O *speckle* é um fenômeno de interferência da luz que retorna de um objeto iluminado por uma luz coerente, fazendo com que a imagem observada seja constituída de áreas como resultado de interferência construtiva e destrutiva, dando origem a grãos claros e escuros.

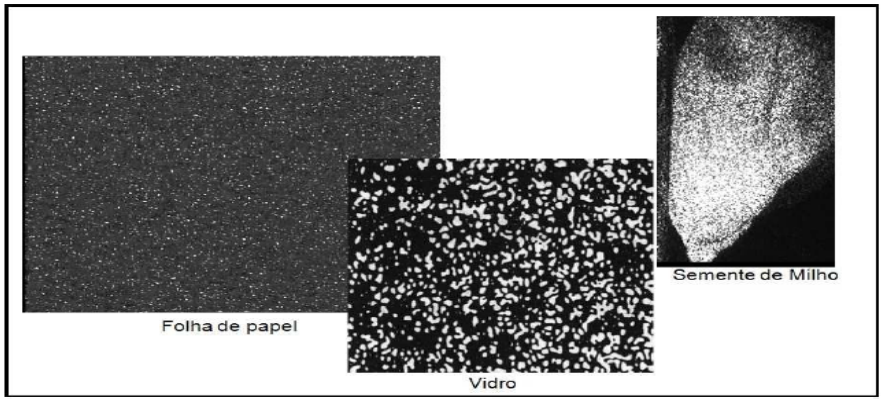

Figura 1 Exemplos de *Speckle*.

Existem aplicações que analisam o *speckle* como informação da

superfície iluminada (SEMENOV et al., 2008), porém, muitas aplicações estão sendo desenvolvidas para o monitoramento da atividade promovida pela mudança da interação da luz no tempo em objetos que apresentam mudanças de posicionamento dos elementos dispersores da luz. A essa linha de trabalho damos o nome de *speckle laser* dinâmico.

2.4 *Speckle* laser dinâmico

O *Speckle laser* dinâmico ou *biospeckle laser* ocorre nos casos em que o material iluminado tem algum tipo de atividade física ou biológica. Essa atividade faz com que os elementos dispersores da luz alterem a sua posição, o que torna o padrão *Speckle* variável ao longo do tempo. No caso de iluminação em materiais biológicos, a atividade biológica fará com que a luz retorne trazendo informação do interior do objeto bem como da área superficial, variando o padrão de interferência de acordo com a movimentação das moléculas, representando assim um padrão de atividade do material. Essa modificação que representa a atividade do material pode ser mais lenta ou frenética. É possível relacionar o *biospeckle* com a vitalidade do tecido, ou seja, quanto mais intensa é a variação no *biospeckle* mais atividade existe no tecido, consequentemente mais vivo é o tecido (BRAGA et al., 2009).

Os princípios ópticos relacionados com o *speckle* dinâmico são, de acordo com Dainty (1975), bem conhecidos em estudos de óptica, e ocorre quando o *laser* se dispersa sobre uma superfície, a qual exibe algum tipo de atividade. De acordo com o princípio de Huygens, quando um feixe de luz atinge uma superfície, cada ponto desta atua como um emissor de ondículas secundárias. No caso em que tal superfície é opticamente rugosa, com os centros espalhadores distribuídos ao acaso, estas ondículas são espalhadas com fases iniciais variando aleatoriamente. Os caminhos ópticos percorridos por estas

frentes de ondas são distintos para cada ponto do plano de observação e a superposição coerente dessas ondas dá origem a um padrão de interferência cujas intensidades variam ao acaso (RABAL; BRAGA, 2008). Nos pontos de interferência construtiva ou destrutiva ocorre a formação de grãos claros e escuros, respectivamente. Tais características conferem caráter estatístico ao granulado óptico, de forma que sua análise segue tratamento semelhante ao dado para o passeio aleatório no plano complexo.

Nos casos em que a superfície do objeto ou meio de propagação introduzem modulações nas ondas espalhadas, o padrão resultante é dinâmico apresentando aspectos de fervilhamento. Tais flutuações nas intensidades são devidas a variações de fase dos diferentes raios interferentes em determinado ponto do plano de observação.

A frequência dos fótons espalhados está diretamente relacionada com as velocidades das partículas. Centros espalhadores mais velozes provocam maiores deslocamentos em frequência e, consequentemente, variações mais rápidas de fase e intensidades. Esse deslocamento é conhecido como efeito Doppler (RABAL; BRAGA, 2008). As diferenças entre frequências provocadas por esse efeito são pequenas (alguns Hertz) e o espalhamento é do tipo quase elástico. Na superposição resultante, ocorre o batimento de frequências. As variações de fase são independentes da direção do movimento das partículas, ou seja, não importa se as ondas são espalhadas a partir de partículas que se aproximam ou se afastam do plano de observação. De acordo com o teorema do limite central, desde que esses movimentos possuam velocidades completamente aleatórias, as frequências são espalhadas em distribuição gaussiana.

O *speckle* dinâmico tem sido uma valiosa ferramenta utilizada para auxiliar na medição de atividades biológicas em diversas áreas do conhecimento como na medicina, na agricultura, na ciência dos alimentos e na medicina veterinária. Na agricultura podemos observar trabalhos que usam o *biospeckle*

em análise de danos em frutos (PAJUELO et al., 2003) e na análise de amadurecimento em tomates (ROMERO; MARTÍNEZ; ALANÍS, 2009), além de diversos trabalhos no estudo da viabilidade de sementes (BRAGA et al., 2003), monitoramento de crescimento de raízes (BRAGA et al., 2009). Existem também diversas pesquisas na área de medicina veterinária e medicina, como a análise de sêmen animal (CARVALHO et al., 2009) e pesquisas com microcirculação sanguínea (GONIK; MISHIN; ZIMNYAKOV, 2002).

Essas aplicações se baseiam no processamento das imagens do material iluminado pelo *laser* com a finalidade de quantificar o nível de atividade no material ou identificar áreas com diferentes níveis de atividade. No primeiro caso, normalmente é utilizada uma análise numérica enquanto no segundo a análise é gráfica.

2.5 Configuração experimental

A observação de fenômeno pode ser realizada em duas configurações distintas. A primeira delas é a chamada propagação em espaço livre, na qual nenhum elemento óptico é colocado entre a superfície espalhadora e o plano de registro. Nessa configuração, geralmente, apenas um ponto da superfície é iluminado por um feixe *laser* e a luz espalhada é registrada em um sensor CCD (Charge-Coupled Device) colocado em um plano distante (RABAL; BRAGA, 2008). A segunda é quando se utiliza lentes para focar o *laser* ou para que toda a amostra seja coberta pelo feixe de *laser*, sendo esse último o caso mais comum.

Para cada tipo de experimento, dependendo dos objetivos, uma configuração experimental diferente é adotada. Contudo, existe certo padrão adotado pela maioria dos profissionais e pesquisadores da área. Para a maioria dos experimentos o *laser* usado para iluminação das amostras é um *laser* estável, de baixa intensidade, geralmente é utilizado o *laser* de HeNe com comprimento

de onda de 632 nm e potência em torno de 10 mW. Uma lente expansora é usualmente utilizada para que o feixe *laser* cubra toda a amostra. As imagens normalmente são capturadas por uma câmera CCD e possuem resoluções bem variadas, geralmente se adota 640x480 *pixels*. A taxa de aquisição de imagens também varia conforme o objetivo, para casos gerais é adotado 0,08s e o tempo de abertura do obturador da câmera é de 1/60s.

As imagens normalmente são provenientes da iluminação das amostras com a configuração experimental baseando-se no *back-scattering*, ou seja, o que se observa é o retorno da luz. Em alguns casos também é adotado o *forward-scattering*. A Figura 2 extraída de Braga et al. (2009) ilustra as duas configurações experimentais.

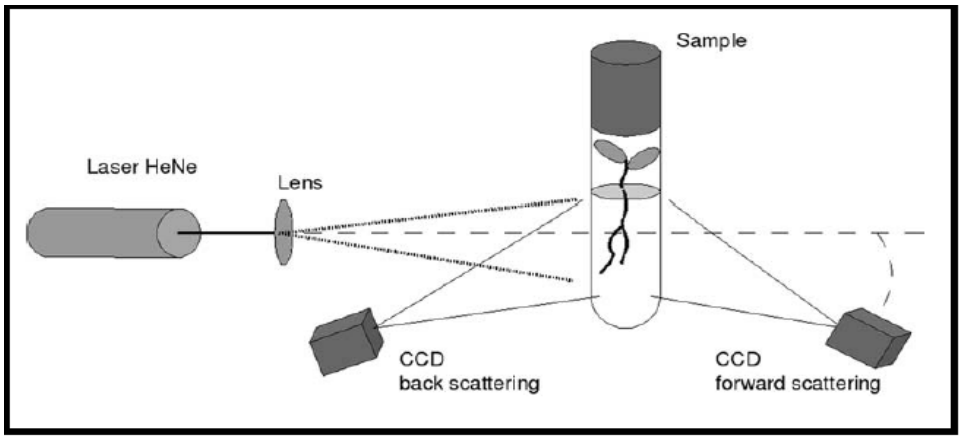

Figura 2 Ilustração para a configuração experimental dos experimentos

2.6 Métodos de análise do *Speckle* dinâmico

São vários os métodos de análise do *speckle* dinâmico, que podem ser divididos em dois tipos: numéricos e gráficos. A análise numérica é recomendada para materiais homogêneos, ou seja, materiais que em todas as suas regiões o nível de atividade é o mesmo, como é o caso nas análises com sêmen animal e em concentração de parasitos em um diluente por exemplo.

Entre os métodos de análise numérica se destacam o Momento de Inércia, o Método do Contraste, e o da Autocorrelação.

As análises gráficas são recomendadas para amostras de áreas heterogêneas em relação ao nível de atividade presente. Na análise do *speckle* dinâmico, as principais técnicas utilizadas são Fujii, Diferenças Generalizadas (DG) e contraste de Briers (também chamado de Lasca) (BRIERS, 1975).

Além disso, a análise espectral tem sido de grande destaque no auxilio de análises convencionais do BSL. A abordagem em frequência pode ser empregada em todas as técnicas de análise descritas acima. Por meio dela, os resultados podem ser filtrados a fim de que possam ser associados com fenômenos específicos que ocorrem nos materiais iluminados. Uma das ferramentas matemáticas mais usadas no caso da análise do *speckle* dinâmico no domínio da frequência é a transformada de *wavelets*.

2.6.1 Momento de inércia

A técnica do Momento de Inércia (MI) é bastante difundida entre os pesquisadores que trabalham com o *speckle* dinâmico. Ela consiste na construção e análise do padrão THSP (*Time History Speckle Pattern*) (ARIZAGA; TRIVI; RABAL, 1999). O THSP é uma imagem bidimensional que representa como uma linha da imagem está variando no tempo. Na aquisição de imagens, cada quadro é capturado a um dado intervalo de tempo. A construção do THSP consiste na aquisição de uma linha na mesma posição das imagens que se denominam participantes, que pode ser uma linha horizontal ou uma coluna, normalmente na região central das imagens para se evitar efeitos de borda. Cada uma dessas linhas é colocada lado a lado e sequencialmente em uma mesma imagem formando o THSP, que possui as dimensões (MxN) em que M é a dimensão da linha, no caso é a dimensão da linha horizontal central das imagens,

e N é o número de imagens utilizadas, ou seja a informação no tempo. A Figura 3 ilustra essa operação nos primeiros 3 passos.

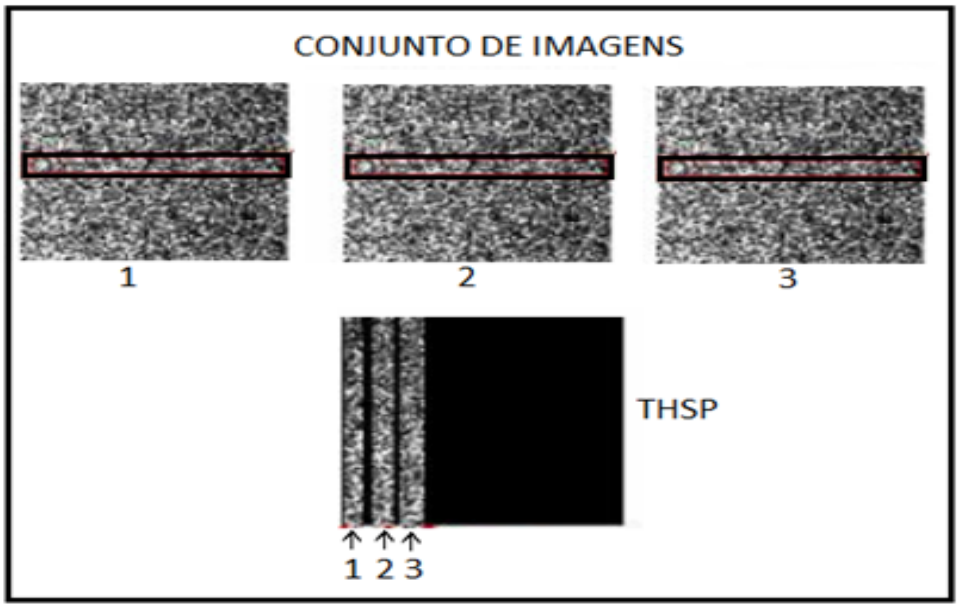

Figura 3 Construção de um THSP

A Figura 3 mostra que cada linha foi transposta se tornando coluna. Normalmente, isso é utilizado a fim de padronizar a imagem, para que o eixo horizontal do THSP esteja representando o tempo e o vertical represente a posição. Pela observação do THSP podemos ver se um *speckle* está variando com muita ou pouca intensidade. A Figura 4a mostra um THSP de um material em baixa atividade e de um em alta atividade (Figura 4b). Nota-se claramente que no material de baixa atividade a linha que uma posição qualquer da imagem tem pouca variação de intensidade ao longo do tempo enquanto no material de alta atividade, a variação de intensidade é intensa.

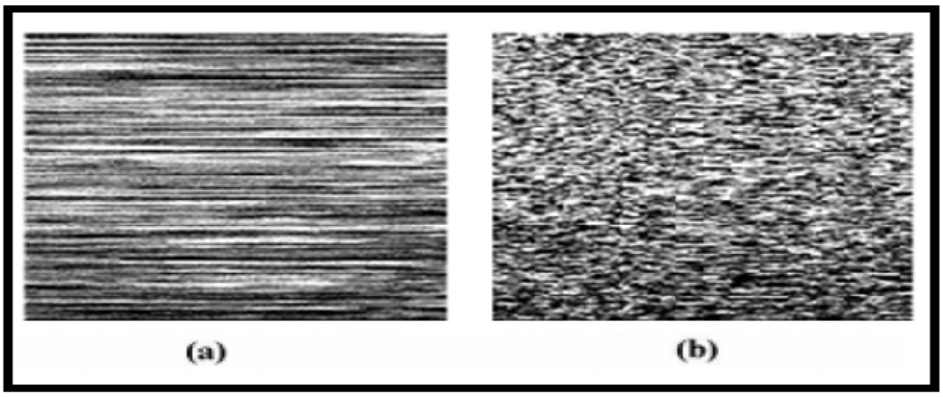

Figura 4 Exemplos de THSP

O tamanho do THSP pode ser ajustado de acordo com a utilidade, sendo que a redução no tamanho representará claramente uma redução da quantidade de dados utilizados para a análise, todavia não significando necessariamente uma perda de informação (BRAGA et al., 2007).

A técnica do MI consiste na quantificação da variação de um THSP e para isso uma matriz de ocorrência (MOC) é construída. A MOC foi proposta por Haralick, Shanmugan e Dinstein (1973) para análise de textura de imagens. Para a análise do *speckle* dinâmico Arizaga, Trivi e Rabal (1999) propôs que a matriz de coocorrência fosse calculada sobre o THSP. A matriz de ocorrência é definida por:

$$MOC = [N\_ij] \quad (1)$$

Em que N_ij é uma matriz de dimensão (MxM) em que o valor de M é o número de valores de intensidade que um *pixel* qualquer possa adquirir quando uma imagem é transformada em uma matriz numérica. Para imagens de 8 *bits*, M é 256, isso porque o *pixel* pode variar de 0 a 255 na escala de cinza. O valor de N_ij corresponde ao número de vezes que o valor de intensidade ‘i’ é seguido

pelo valor ‘j’, sendo que ‘i’ e ‘j’ variam de 1 a 256 para imagens de 8 bits.

Considere uma situação em que a codificação de tons de cinza seja realizada com apenas 2 *bits*, resultando em uma resolução de 4 tons de cinza. Na Figura 5 temos essa representação ilustrando um caso de material com baixa e com alto nível de atividades. As imagens à esquerda correspondem aos THSP’s hipotéticos. Na sequência, temos as respectivas matrizes numéricas com os níveis de intensidades desses THSP’s e, logo em seguida, as matrizes de coocorrência onde cada elemento traz o número de vezes que o nível de cinza ‘i’ foi seguido do nível de cinza ‘j’. Por fim, à direita tem-se as imagens MOC's, onde os valores nulos são representados por *pixels* pretos e os valores não nulos, por *pixels* cinza-claro à brancos.

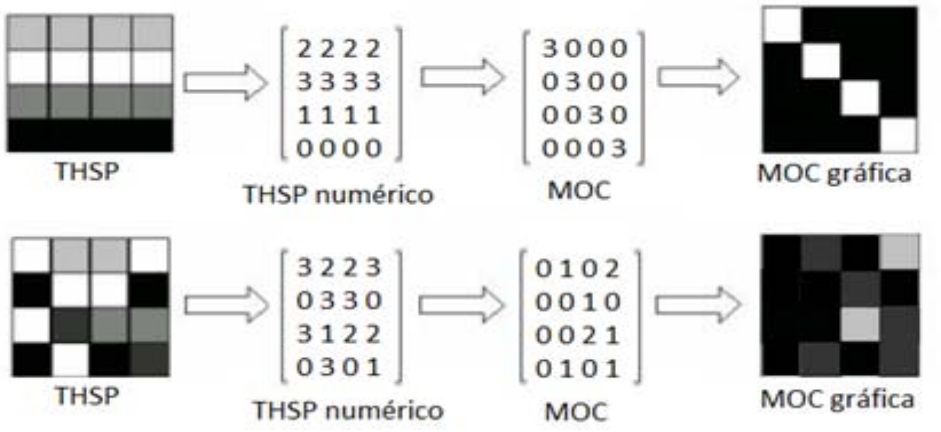

Figura 5 Exemplo ilustrativo para cálculo de uma MOC em um THSP de material pouco ativo (acima) e um material mais ativo (abaixo)

A característica de uma MOC para um material iluminado, totalmente estático, apresenta apenas a diagonal principal com valores não nulos de ocorrências uma vez que o THSP praticamente não tem variações de intensidade ao longo do tempo como na Figura 4(a). Por outro lado, quando o THSP apresenta grande atividade (como na Figura 4(b)), os elementos não nulos se espalham ao redor da diagonal principal. Assim, quanto mais ativa a amostra,

mais dispersos em relação à diagonal se distribuem os pontos.

A Figura 6 representa uma sequência de THSP's com as respectivas MOC's. Na Figura 6(a) temos a situação gerada a partir do espalhamento de luz por uma superfície praticamente inativa, e Figura 6(c) está associada a uma superfície com elevado grau de atividade, enquanto que na Figura 6(b) os valores correspondem a níveis intermediários.

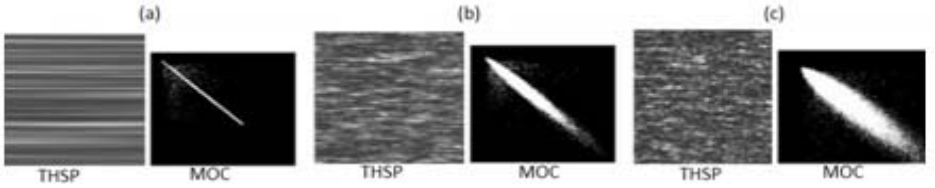

Figura 6 Exemplos de THSP e suas MOC's correspondentes

O Momento de Inércia (MI) é chamado assim como uma analogia ao momento de inércia da mecânica, devido à semelhança de suas fórmulas. Também é chamado de momento de intensidades ou simplesmente de nível de atividade.

O MI é calculado como sendo a distância de cada ponto da MOC até a diagonal principal multiplicada pelo peso de cada ponto, que representa o número de ocorrências. A Equação 2 expressa essa ideia:

$$MI = \sum_{i,j} M_{ij} (i - j)^2 \qquad (2)$$

Em que, é uma normalização fazendo com que o valor de cada linha na MOC seja igual a 1. Matematicamente temos:

$$M_{ij} = \frac{N_{ij}}{\sum_i N_{ij}} \qquad (3)$$

Em que é o número de ocorrência na posição (i,j). Assim quanto maior o MI mais ativo está o material iluminado, sendo que este parâmetro tem sido utilizado em diversas análises que envolvem o *speckle* dinâmico.

2.6.2 Fujii e diferenças generalizadas

Os métodos de Fujii e DG são comumente usados para análise gráfica do *speckle* dinâmico. O método de Fujii (1985) baseia-se no cálculo da visibilidade entre os *pixels* de imagens gravadas ao longo do tempo. O procedimento para a construção do método de Fujii ocorre segundo a Equação 4.

$$\mathrm{Fujii}(x,y) = \sum_{k=1}^{N} \frac{I_k(x,y) - I_{k+1}(x,y)}{I_k(x,y) + I_{k+1}(x,y)} \qquad (4)$$

Em que, é o valor de intensidade na posição da imagem k. O denominador representa uma ponderação que aumenta a intensidade de áreas mais escuras da imagem. A fim de se fazer a análise gráfica de um conjunto de imagens que representem a variação de um material ao longo do tempo, por meio da técnica de Fujii, as diversas imagens são transformadas em matrizes numéricas. O valor numérico de cada *pixel* nas posições representa a sua intensidade em uma escala de tons de cinza, podendo variar de 0 a 255.

A partir da equação acima uma nova imagem é construída. Assim os *pixels* assumem no mapa final um valor próximo de zero, na escala de tons de cinza, em regiões onde não houve alterações de intensidade ao longo do tempo, e valores mais altos, próximos de 255, em zonas em que os *pixels* sofreram grandes alterações. Dessa maneira, nas zonas de grande atividade a imagem resultante apresenta pontos claros e naquelas áreas de baixa atividade os *pixels*

apresentam pontos escuros.

O método de Diferenças Generalizadas (DG) é uma técnica derivada do método de Fujii sem o denominador, que pondera a somatória das diferenças e, que neste caso ainda apresenta uma comparação generalizada entre imagens, ou seja, cada imagem é comparada com todas as outras, e não somente com a subsequente como no caso do Fujii. De acordo com Arizaga, Cap e Rabal (2002), o que se faz, então, é realizar uma soma das diferenças de intensidade entre uma imagem e as suas subsequentes. A Equação 8 apresenta o modelo matemático que descreve o método de DG. O resultado é uma nova imagem, em 8 *bits*, com a distribuição espacial da atividade. Assim como no método de Fujii, a imagem resultado apresentará *pixels* com valor próximo de 225 em áreas de alta atividade e *pixels* próximos de 0 em regiões de baixa atividade.

$$DG(x,y) = \sum_{k=1}^{N} \sum_{l=1}^{N} I_k(x,y) - I_{k+l}(x,y) \qquad (5)$$

Na técnica de Fujii, a divisão (ou ponderação) da diferença entre as intensidades pela soma das intensidades entre uma imagem e sua subsequente faz com que áreas escuras nas imagens participantes se tornem mais claras no processamento, o que em termos práticos significa que áreas com baixos níveis de intensidade também participem da imagem final, deixando de ser um método linear. Em contrapartida, na técnica de DG apenas as altas variações são valorizadas. Outra diferença observada é o tempo de processamento da técnica de DG ser muito maior por conta da necessidade da generalização das diferenças.

A Figura 8 ilustra um conjunto de imagens de uma semente de milho conhecido como conjunto de imagens participantes, que é o resultado da captura destas imagens ao longo de um período com a semente, iluminado por um feixe *laser* expandido. A Figura 9 demonstra o resultado do processamento usando

Fujii e DG para as imagens participantes da Figura 8.

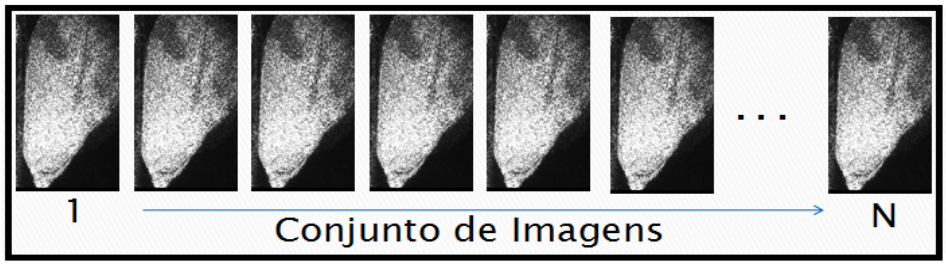

Figura 8 Conjunto de imagens de milho

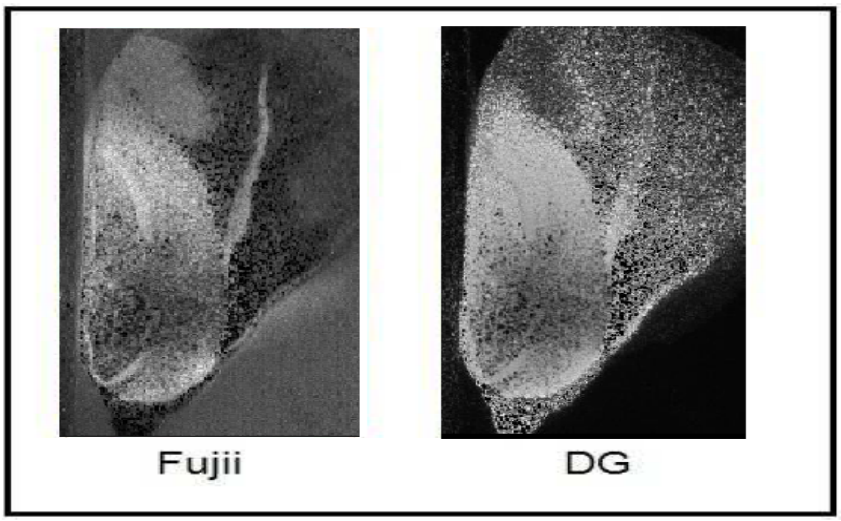

Figura 9 Processamento de Fujii e DG para o conjunto de imagens participantes de semente de milho

Pode ser observado nas imagens de Fujii e DG que o embrião fica mais destacado do que o endosperma, isso porque a atividade na região embrionária é maior. Nota-se também que a mesa, no processamento de Fujii, fica mais clara do que no DG, isso devido à ponderação da técnica de Fujii que intensifica regiões mais escuras.

2.6.3 Transformada de Wavelets aplicada à análise do BSL

A abordagem em frequência do speckle dinâmico pode ser empregada em todas as técnicas de análise descritas acima. Por meio dela, os resultados podem ser filtrados a fim de que possam ser associados com fenômenos específicos que ocorrem nos materiais iluminados. Uma das ferramentas matemáticas mais usadas no caso da análise do speckle dinâmico no domínio da frequência é a transformada de wavelets.

A transformada de wavelets tem sido utilizada para analisar o speckle dinâmico no domínio da frequência tanto por análises numéricas quanto por gráficas. Nas análises numéricas estudos feitos por Nobre et al. (2009) mostraram que o momento de inércia tem um funcionamento limitado à alta frequência. Nesse sentido Braga et al. (2011) têm sugerido um novo método para o cálculo do MI a fim de corrigir essa deficiência. Passoni et al. (2005) fizeram várias análises usando a transformada de wavelets em associação a entropia em análises de diversos materiais. Porém Nobre et al. (2009) mostraram que a técnica de entropia é limitada à baixa e média frequência. Outros estudos como os de Amalvy et al. (2001) utilizam a abordagem em frequência juntamente com técnicas numéricas de análise do speckle dinâmico e técnicas de interferometria.

Sendra et al. (2005) mostraram a aplicação da técnica de análise em frequência juntamente com técnicas de análise gráfica, neste caso usando filtros butterworth. Um exemplo da análise no domínio da frequência é o trabalho com sementes apresentado por Cardoso et al. (2011) e o trabalho com raízes em cultura de tecidos de Braga et al. (2009) que utilizaram a técnica para diferenciar as áreas mais ativas e encontrar a frequência com que certos fenômenos no material atuam.

A Figura 15 a seguir, exemplifica essa técnica, onde a transformada de wavelets foi aplicada pixel a pixel, sendo que cada imagem é resultado do processamento de Fujii em um conjunto de 128 imagens que foram

reconstruídas em uma banda de frequência específica. À direita está a imagem de referência a qual não foi processada com wavelets.

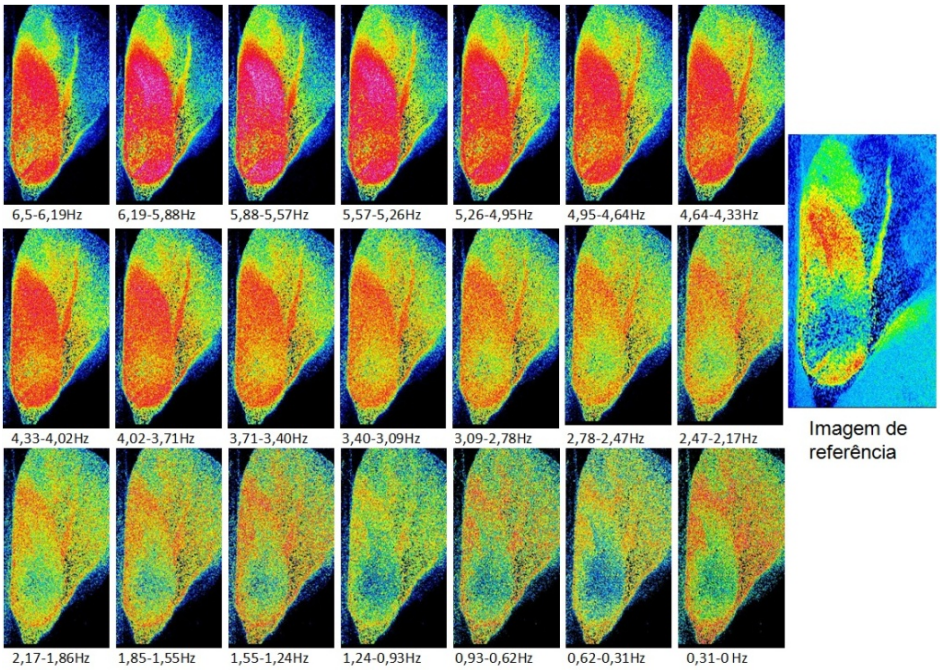

Figura 15 Resultado do processamento usando wavelets para semente de milho (CARDOSO et al., 2011)

Tanto na análise numérica quanto na gráfica, a faixa máxima de frequência que podemos visualizar está relacionada com a taxa de aquisição de imagens pelo teorema da amostragem. No caso da taxa de 0,08 seg. a frequência máxima é 6,25 Hz. O número de bandas de frequência que se pode ter está relacionado com o número de imagens. No caso de 128 e 64 imagens, temos um total de 25 e 21 bandas de frequência respectivamente.

2.7 Qualidade de imagem do speckle

As técnicas de análise do speckle dinâmico tem sido de grande utilidade em diversas áreas do conhecimento, como na agricultura, medicina veterinária,

ciência dos alimentos entre outros. As aplicações são inúmeras e o desenvolvimento dessa ferramenta possibilita grandes inovações e avanços.

Contudo, em várias aplicações das metodologias e técnicas descritas acima uma das barreiras é a alta sensibilidade do speckle dinâmico acarretando muitas vezes redução na qualidade do sinal, que neste caso é representado pelo grão do speckle se deformando no tempo. A variação na qualidade do sinal causa uma baixa repetibilidade nos resultados diminuindo a confiabilidade da ferramenta, e desta forma, vários trabalhos têm sido feitos para solucionar esse problema.

Nesse caso o controle é feito na configuração experimental. Em outros trabalhos como os de (BRAGA et al., 2008; SKIPETROV et al., 2010) o controle dos ruídos é feito no processamento dos dados. No trabalho de Skipetrov et al. (2010) é feita a correlação do ruído verificando se existe alguma coerência no seu comportamento.

A demanda por novos trabalhos nesse sentido ainda é alta, a fim de validar completamente a técnica do speckle dinâmico como instrumento óptico aplicado.

3 CONCLUSÃO

As metodologias e técnicas apresentadas incrementam e melhoram os procedimentos clássicos de análise do BSL. Em particular, a abordagem em frequência possibilitou a marcação em frequência de fenômenos específicos em sementes, como a atividade embrionária e atividade relativa à água. As análises numéricas associada às análises gráficas tornou mais precisa a diferenciação e assinatura espectral entre tecidos diferentes em um mesmo material.

O protocolo usado para avaliar a qualidade de imagem do BSL durante a iluminação apresenta grande destaque por reduzir o subjetivismo e garantir análises mais seguras e confiáveis. A normalização proposta da técnica do MI reduz a alta dispersão entre repetições, o que garante uma análise numérica mais coerente e precisa.

A técnica de MI contínuo permitiu acompanhar um fenômeno no tempo identificando uma mudança em um momento, podendo ser utilizada para detectar variações bruscas de atividade em curto espaço de tempo no BSL. A técnica do desvio padrão gráfico apresentou velocidade de processamento baixo e boa qualidade da imagem final, viabilizando o seu uso como ferramenta gráfica de análise do *speckle* dinâmico.

REFERÊNCIAS

AMALVY, J. I. et al. Application of dynamic speckle interferometry to the drying of coatings**. Progress in Organic Coatings**, Fargo, v. 42, p. 89-99, 2001.

ARIZAGA, R.; CAP, N. L.; RABAL, H. Display of local activity using dynamical speckle patterns**. Optical Engineering**, Bellingham, v. 4, n. 2, p. 287-294, 2002.

ARIZAGA, R.; TRIVI, M.; RABAL, H. J. Speckle time evolution characterization by the co-occurrence matrix analysis. **Optics & Laser Technology**, Benevento, v. 31, p. 163-169, 1999.

BRAGA, R. A. et al. Assessment of Seed Viability by Laser Speckle Techniques. **Biosystems Engineering**, London, v. 86, p. 287-294, 2003.

BRAGA, R. A. et al. Evaluation of activity through dynamic laser speckle using the absolute value of the differences. **Optics Communications**, Sydney, v. 284, p. 646-650, 2011.

BRAGA, R. A. et al. Live biospeckle laser imaging of root tissues**. European Biophysics Journal**, Berlin, v. 38, n. 5, p. 679-86, 2009.

BRAGA, R. A. et al. Reliability of biospeckle image analysis. **Optics and Lasers in Engineering**, Lausanne, v. 45, p. 390-395, 2007.

BRAGA, R. A. et al. Time history speckle pattern under statistical view. **Optics Communications**, Sydney, v. 281, p. 2443-2448, 2008.

BRIERS, J. D. Wavelength dependence of intensity fluctuations in laser speckle patterns form biological specimens. **Optics Communications**, Sydney, v. 13, p. 324, 1975.

CARDOSO, R. R. et al. Frequency signature of water activity by biospeckle laser. **Optics Communications**, Sydney, v. 285, p. 2131-2136, 2011.

CARVALHO, P. H. A. et al. Motility parameters assessment of bovine frozen semen by biospeckle laser (BSL) system. **Biosystems Engineering**, London, v. 102, p. 31-35, 2009.

DAINTY, J. C. Statistics of normal and anomalous speckle patterns. **Journal of the Optical Society of America**, New York, v. 65, n.10, p. 1190-1190, 1975.

FACCIA, P. A. et al. Differentiation of the drying time of paints by dynamic speckle interferometry. **Progress in Organic Coatings**, Fargo, v. 64, p. 350-355, 2009.

FUJII, A. H. Blood-flow observed by time-varying laser speckle. **Optics Letters**, Washington, v. 10, n. 3, p. 104-106, 1985.

GONIK, M. M.; MISHIN, A. B.; ZIMNYAKOV, D. Visualization of blood microcirculation parameters in human tissues by time-integrated dynamic speckles analysis. **Annals of the New York Academy of Sciences**, New York, v. 972, p. 325-330, 2002.

HARALICK, R. M.; SHANMUGAN, K.; DINSTEIN, I. Textural Features for Image Classification. **IEEE Trans. Systems, Man and Cybernetic**s, New York, v. 3, n. 6, p.610-621, 1973.

NOBRE, C. M. B. et al. Biospeckle laser spectral analysis under Inertia Moment, Entropy and Cross-Spectrum methods. **Optics Communications**, Sydney, v. 282, n. 11, p. 2236-2242, 2009.

PAJUELO, M. et al. Bio-speckle assessment of bruising in fruits. **Optics and Lasers in Engineering**, Lausanne, v. 40, p. 13-24, 2003.

RABAL, H. J.; BRAGA, R. A. Dynamic laser speckle and applications. New York: CRC Press, 2008.

RABELO, G. F. **Avaliação da aplicação do "Speckle" dinâmico no monitoramento da qualidade da laranja**. 2000. 149 p. Tese (Doutorado em Engenharia Agrícola) - Universidade Estadual de Campinas, Campinas, 2000.

ROMERO, G. G.; MARTÍNEZ, C. C.; ALANÍS, E. E. Bio-speckle activity applied to the assessment of tomato fruit ripening. **Biosystems Engineering**, London, v. 103, p. 116-119, 2009.

SEMENOV, D. V. et al. Statistical properties of dynamic speckles formed by a deflecting laser beam. **Optics Express**, Washington, v. 16, n. 2, p. 2906-2912, 2008.

SENDRA, G. H. et al. Decomposition of biospeckle images in temporary spectral bands. **Optics Letters**, Washington, n. 30, n. 13, p.1641-1643, 2005.

SKIPETROV, S. E. et al. Noise in laser speckle correlation and imaging techniques. **Optics Express**, Washington, v. 18, n. 14, p. 14519-14534, 2010.

TCHVIALEVA, L. et al. Surface roughness measurement by speckle contrast under the illumination of light with arbitrary spectral profile. **Optics and Lasers in Engineering**, Lausanne, v. 48, n. 7/8, p. 774-778, 2010.

SEGUNDA PARTE – ARTIGOS

ARTIGO 1 Frequency signature of water activity by biospeckle laser

Rafael Rodrigues Cardoso, Anderson Gomide Costa, Cassia Marques Batista Nobre, Roberto Alves Braga Jr

Esse artigo foi publicado no periódico Optics Communications no volume 284, páginas 2131 a 2136 em Janeiro/2011. O artigo está no formato em que foi publicado.

ABSTRACT

Biospeckle laser technique has become an important tool to investigate biological activity in severa I areas of science. However. due to the complexity of biological materiais it is necessary to develop research processes that ensure greater efficien'Cy l'n isolating areas of different activities in the same material using the biospeckle. Thus. alternarive techniques. such as those related to spectral domain. allow approaches that provide a means for frequency and isolation marking of various observed phenomena. The possibility of creating frequency markers related to physical or chemical phenomena under biospeckle laser monitoring opens the way for important applications in the analysis of biological materiais. In seeds. for exarnple, one research challenge is the creation of a methodology to analyze their vigor undermining the influence of water activity. This study aimed to use wavelet transform to create maps in frequency of biological material. particularly frorn maize and bean seeds, seeking to isolate water activity. Wavelet transform was used in conjunction with traditional biospeckle laser methods. Fujii. Generalized Differences and Time History Speckle Parrerns. The data analysis allowed access of information in different frequencies. making it possible to map activities that only occur ar certain frequencies in the seeds associated to particular areas they opera te. as in the case of activities presenr in the ernbryo as well as those present in the endosperm. Thus the work enabled the identification of frequency bands where water activiry may be operating creating a signature useful in further works.

1 INTRODUCTION

Methods of analysis which use non-destructive techniques have been of great importance in the evaluation and monitoring of biological properties. That's why biospeckle laser (BSL) has become over the years an increasingly efficient application for monitoring activity. particularly in the areas of biology, medicine and agriculture [1]. In agriculture, we find works that use BSL in fruit analysis [2], in seed and fungi analysis [3,4], in leaves of coffee moisture monitoring [5], in root growing observation [6] and in works with animal semen evaluation [7]. The biospeckle technique. also known as dynamic laser speckle, is based on monitoring changes in interference patterns prominent from iIIumination over time by a coherent Iight, in particular the laser [8]. The changes mentioned before are related to the movement of dispersors of Iight which can be either within the cells or externa I of them. In most cases, the water content, or water activity, will be one ofthe main contributors ofthe levei ofactivity [9]. The routine methods proposed to analyze the activity through BSL technique are based on the summation of ali contributions related to a wide range of phenomena, thus without the ability to separate or isolate a particular feature [10]. There are many approaches to achieve the final result of the multiple interferences expressed by the BSL. and they can be divided in on-line and off-line techniques. The on-line techniques are based on the single-exposure speckle photography [11,12], also known as Laser Speckle Contrast Imaging field (LSCI). The alternatives to the absence of the time history are presented by the Time Laser Speckle Contrast Imaging field (TLSCI), also known as Laser Speckle Temporal Contrast Analysis (LSTCA) [13], or in the field ofthe off-Iine techniques which are mainly discussed in this work. The great Iimitation of not being able to access the final activity without the identification ofthe main contributors demanded alternative ways to split the original signal into

subsignals which can be linked to any particular feature or even to enhance the results by avoiding or damping some undesirable information. One case of splitting separated the levels of grey scales in the irnages by means of three thresholding ranges through fuzzy approaches [141. Another way to go further into the separatíon of signals adopted spectral ranges as a feasible alternative [151. which was improved by the use of the wavelets transforrn [16,17]. and with the implementation of Entropy as an alterna tive to Inertia Moment [17]. The adoption of the CrossSpectrum theory was an additional tool in the spectral domain [18], which was compared to the Inertia Moment and Entropy [19] regarding the frequency point ofview.lt was presented that Entropy and Cross-Spectrum offered better answers for low frequency components in the original signal while lnertia Moment was better with high frequency components. The huge absence of time information in the LSCI or even the low amount of images in the LSTCA is the rnain Iimitation to these techniques to the adoption of the spectral approaches. The challenge of isolation [1 O] was in turn a great motivation in this field with many relevant applications. in particular in the seed analysis area where it is possible to see many efforts to deal with it using digital imaging information technology [20]. This work aimed to present steps to achieve actual isolation of biological phenomena by means of spectral approaches associating them to graphical and numerical routine methods.

2 THEORY

2.1 Graphical analysis of the biospeckle

Among the routine methods to analyze graphically the biospeckle one can highlight the Fujii approach [21] and the Generalized Oifferences Method [22]. Fujii's method is based on the visibility caJculation among the pixels of images recorded ave r time. The procedure for the construction of the Fujii method is described by Eq. (1).

$$I(x,y) = \sum_{k} \left| \frac{I_k(x,y) - I_{k+1}(x,y)}{I_k(x,y) + I_{k+1}(x,y)} \right| \qquad (1)$$

where *Ik(X,y)* is the intensity value at image *k* and position *(xJ').* From Eq. (1) a new image is constructed, and the pixels assume in the final map a value dose to zero on the gray shades scale in areas where there were no changes in intensity ave r time. and higher values. near 255 in areas where the pixels went through big changes. The Generalized Oifference Method (GO) is a derivative technique from the Fujii method without the denominator and with a recursion on the differences. In the GO. what is done is to perform a sum of intensity differences between an image and its subsequent. The resulting image can be expressed by Eq. (2).

$$I(xJ') = \boldsymbol{L}\ \boldsymbol{L}\ I/k(X,y) - lk + ,(xJ')1 \qquad (2)$$

where *k* and *I* are the numbers of the images in the image series. The double summation demonstrates one difference in the Fujii method which in this case each image is compared with ali the others. requiring more computational effort.

2.2 Numerical analysis Df biDspeckle

An approach to numerically analyze the images of a tissue from laser iIlumination consists in the creation of the Time History Speckle Pattem orTHSP. The construction ofTHSP was proposed from a pseudotemporal image concepr [23] and from a space-time speckle [24]. The standard THSP is formed when only one row or column is repeatedly captured in the speckle images at a certain sampling rate and then these strips are placed side by side forming a new image. With THSP it is possible to estimate the degree of activity of an illuminated object based on dynamic speckle behavior. Most ofthe techniques described in existing literature are based on obtaining a single numeric value from THSP. This value can be obtained by applying auto-correlation, or through the Inertia Moment (1M) [25]. which results in a second-order statistic. Inertia Moment (1M) values are obtained from the creation of a cooccurrence matrix that is defined by Eq. (3)

$$COM = \left[N_{ij}\right]. \tag{3}$$

Where Nu is the number of occurrences of the gray levei $\mathbf{i}$ followed by the gray levelj over the time dimension in the matrix THSP. where COM is a matrix of 256 x 256. The Inertia Moment values are defined by Eq. (4).

$$IM = \sum_{i}\sum_{j}\left(\frac{N_{ij}}{\sum_{j} N_{ij}}\right) * (i-j)^2. \tag{4}$$

2.3 Spectra/ entropy

Spectral entropy can be obtained from the Fourier power spectrum,

which is a way to verify the order of a signal. i.e, A system that possesses periodicity exhibits a peak in the frequency-domain. Therefore the frequency range (band) concentration in a single peak corresponds to low values of entropy. On the other hand, non-regular activities provide spectral components over a wide range of the frequency-domain. resulting in high entropy [17]. Transformation of the signal to the frequency-domain can be performed directly by the Fourier transformo or specifically by the wavelet transform that allows more information about the frequenàes in time. By using Discrete Wavelets Transform to study the biospeckle. the lines ofTHSP are divided in temporal windows and the wavelets average energy can be obtained from Eq. (5) [17].

Formula 5

where:

i = 1 ..... NT. and NT = signal length/L, which is the size of the temporal window.

N/ number ofWavelet coefficients atj levei of resolution. including i time interval.

The total energy in the i time interval can be obtained by Eq. (6). being that the Wavelets energy pertaining the ith window at the THSP line can be obtained by Eq. (7). and the Shannon entropy at the ith window by Eq. (8). [17].

Formula 6,7 e 8

3 MATERIAL AND METHODS

3.1 Backscattering configuration

The experimental configuration adopted was the backscattering as presented in Fig. 1. where the computer was responsible for assembling the images from the eco camera with a time rate of acquisition set up in 0.08 s. The maximum frequency that could be observed, based on the sampling theory, was 1/(2xO.08)s which was related to 6.25 Hz. The number of frames assembled varied in the experiments but ali of them were expressed in base of 2, in particular 64 and 128 frames, in order to implement the fast fourier transform algorithm.

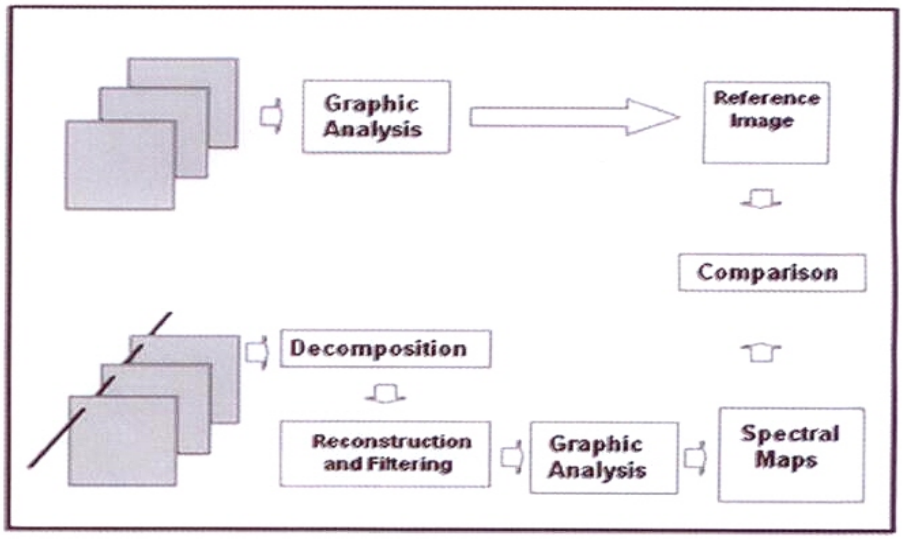

Figura 1 Experimental setup for seed lighting.

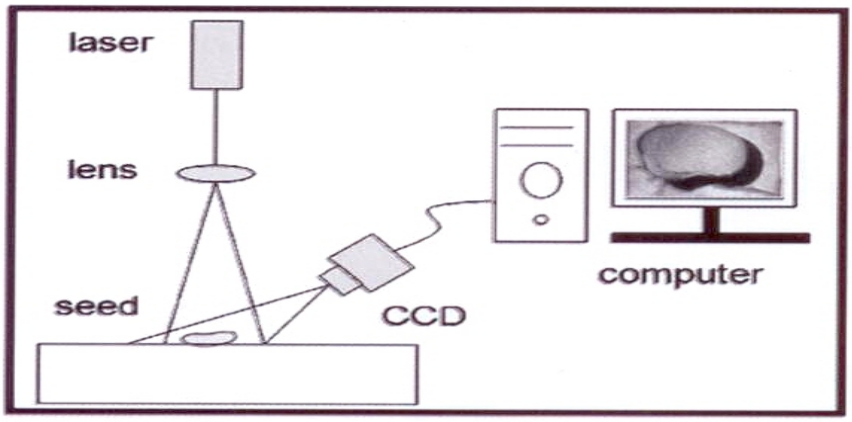

Figura 2 Flowchart representing the analysis with filtering processo

3.2 lIIuminated samples

The biological materiais chosen to be illuminated were bean and corn seeds. The corn seeds had moisture over 20% ofwet base and the bean seeds with different levels of moisture, as well as in two biological stages, one collection alive and another dead. The bean seeds were tested in accordance with their viability and a dead parcel was separated from a Iiving parcel. Both the dead and living seeds were put in wet paper for 12 h and then they were letloose in water at room temperature.

3.3 Graphical analysis

The graphical analysis was conducted in two ways. One was when routine methods, such as GD and Fujii, were implemented without any processing of the original images and the second way was when routine methods were implemented in the collection of primary images after the filtering processo The two filtering processes implemented damping of one range per

time and reconstructing the image, and damping ali the ranges except one which was used as the base for the reconstruction of the resulting image. In Fig. 2 it is possible to see the two paths followed in the graphical analysis. The graphical analysis was implemented in the corn and bean seeds. The protocol of filtering used the wavelets transform [6J and the number of frequency ranges varied in accordance to the number of images assernbled. The inverse wavelet transform was performed in two ways to reconstruct the images: reconstructing the images on just one frequency bando and reconstructing the images by eliminating only one frequency bando For the maize seed, 64 images of256 x 490 pixels were used and it was possible to obtain results in 21 frequency bands between O and 6.25 Hz. For the bean seeds. 128 images of 486 x 469 pixels were used.ln turn, the reconstruction ofthe images to generate spectral maps was performed in order to reconstruct the images on just one frequency band at a time. From the 128 original images, it was possible to obtain 25 frequency bands between O and 6.25 Hz.

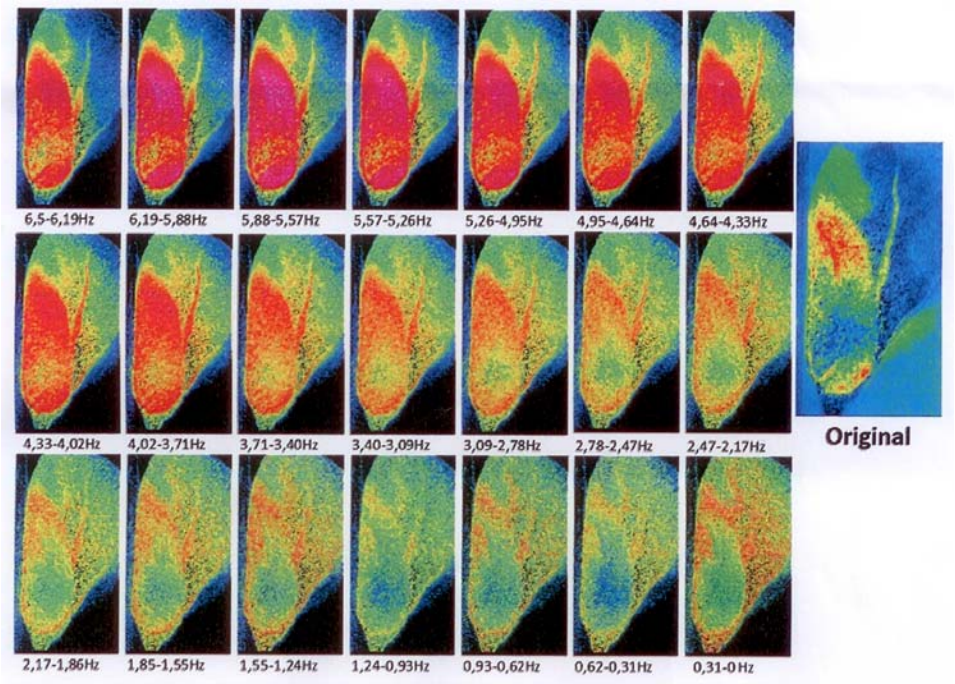

Figura 3 Results of Fujii in maize seeds with filtering reconstructingjust one frequency range. with the larger image on the right representing the image control without any filtering.

3.4 Numerical analysis

THSP live bean seeds were analyzed in two different stages, one which we will call the initial stage where the seed is saturated with water and the other referred to as the final stage where the seed reached hygroscopic equilibrium with the environment. We sought to evaluate the behavior of water activity from the initial stage to final stage. Inertia Moment and Entropy techniques associated with wavelet transform were applied for ftItering and reconstruction of the data. The frequency bands were rejected one by one and then compared to the original not rejecting any frequency range.

4 RESULTS AND DISCUSSIONS

4.1 Graphical analysis

Fig.3 shows the result of processing the method of Fujii in maiz . seed with filtering and reconstruction of only one frequency bando The image control on the right in Fig. 3 represents the result ofthe process without any filtering, where on the bottom left of the seed, the embryo is found with activities represented by the colors red and yellow, and on the top right of the seed, the endosperm is found with low activity represented mainly by blue and green colors. The 21 frequency bands, presented in the first images, show the embryo evidenced in red, which means high activity at high frequencies, while in the last images the endosperm is highlighted in red at low frequencies as was also shown in an earlier work [15]. The use of only one band for the Fujii processing shows that the phenomena that constitute the biospeckle are selectíve, in other words, they are restricted to narrow bands of frequency improving phenomena isolation. opening up a potential application in many biological materiais that demand isolation areas of activity. The observed activity in the endosperm can be attributed to the presence of water in tissue without biological activity. This isolation of water activity in the observed data in the biospeckle is of great relevance to the improvement of the results of seed analysis once the activity promoted by the water in tissue masks the observation of metabolic activities of tissues that makes it difficult to compare and identify living and dead tissues. The separation of the results of Fujii in various frequency ranges allow for isolated forms of observation of the phenomena that are not possible in the original image. An example of this ability is observed in the embryo where at low frequencies a welldefined area of low activity is observed in the center of the embryo, which does not occur at high frequencies showing that in the

original image·the result undermined this information. In turn, the obtained results by eliminating only one frequency band showed no difference from the original image not presented here graphically. This is due to the fact that only one frequency band is not able to alter the final results due to its low energy which is not perceived by processing Fujii, especially in visual formo In the presented results in Fig, 3, it is still possible to observe that there is a range of activity in the endospenn in the central part of the image represented by an active band, in yellow, in the original image processed. This band is related to a crack in the endosperm, and thus a greater activity in this area, where there should normally be less activity, which can be attributed to greater water evaporation. From the images in frequency it is possible to conclude that evaporation in greater activity areas generates high frequency answer in the speckle patterns, showing the signature in frequency of the evaporation phenomenon. The mapping of a bean seed where there is no such clear separation from the embryo and endosperm, as occurs in the com seed, is shown in Fig. 4 reconstructing only one frequency bands. The result shows an area in the seed that operates at a higher rate in the high frequency bands that are related to a portion of the seed attached to higher biological activity during germination. The control image, without any filtering, is in the right of Figura 4. It was also noted that there is some phenomena occurring in ali seeds from the medium to the lowest frequencies, which is related to the water activity characterized as a signature in frequency which is also seen in the corn. To confirm this hypothesis, and seeking separation of water activity in relation to the cellular activity, the numerical analysis occurred with the THSP's bean seed combining the 1M techniques and entropy with spectral analysis.

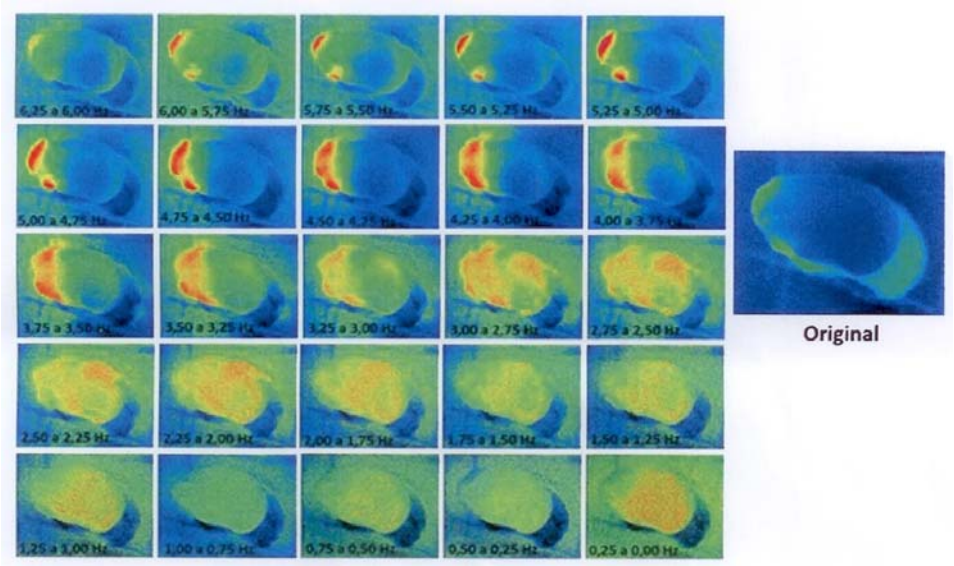

Figura 4 Partial result obtained with the bean seed with mechanical damage, with image control on the rigth

4.2 Numerical analysis

The numerical analysis that showed best results were those in which the reconstructions were based on theelimination of only one frequency band opposing the achieved ones in the graphical analysis. Our ability to analyze numerical values more efficiently than images, and the different routine techniques of graphic and numeric processing. may explain the difference in the reconstruction approach.

4.2.1 Encropy

In Fig. 5 we analyze the behavior in living and dead bean seeds in their initial stage, in other words, with high water activity and then finally with low water activity. As already evidenced, [191 entropy is only able to monitor

changes in speckle patterns related to low frequencies, which in Fig. 5 represent the bands below 3.41 Hz. Entropy behavior, in both living and dead seeds in stages ofhigh water activity and low water activity, is the same at low frequencies, which shows that in these frequency bands only the water is capable of expressing changes in speckle patterns.ln Fig. 5 it is possible to notice a clear separation of entropy in the initial stage of higher water activity in relation to the final stage where the present water in the seed is already in small quantities. In this case, lower entropy observed in the stages of lower water activity is related to phenomena with greater stability, in other words,less random activity, which is directly related to the mobility that water gives to the member components of plant tíssue.and nor to the evaporation. The entropy change, in the bands of 3.41 Hz to 0.0 Hz, can be linked to the type of chemical bond that the water has, but their classification still remains a challenge. Finally, in Fig. 5, it is possible to observe that the entropy differences of live and dead seeds are small, at low frequencies, which leads us to conclude that the biological activity is not relevant in the speckle patterns changes in this spectral bando These achievements are an advance to that presented in other account [10] using the same data. However, in this work the access to the signatures was only possible since the graphical analysis were combined to the numerical answers. In addition, in this work, the whole picture was formed by the adoption of the concepts of absorbed, solvent, adsorbed and constitution water in order to correlate them to the frequency behavior.

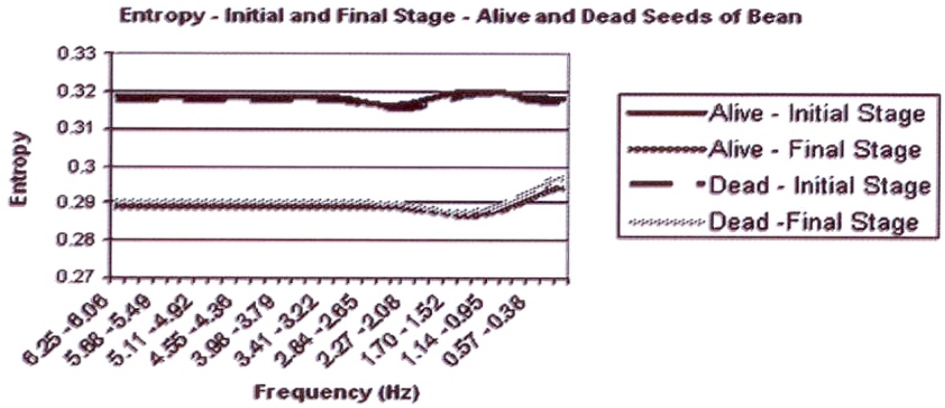

Figura 5 Behavior of entropy in living and dead seeds with high and low water activity

4.2.2 Inertia moment

In Fig. 6 you can notice that by removing the frequencies located in the high frequency band there is a reduction of activity in the seed, occurring sharply in the initial stage when the water concentration is greater inside of it, and occurring less sharply in the final stage when the water concentration is lower inside the seed. We relate this phenomenon to water loss during evaporation as the biological activity ofthe seed itself, as also noted in the corn seed, in particular in the region of the crack, as being more conducive to more intense evaporation. This phenomenon is linked to high frequencies, which explains the greater attenuation observed. In inverse form of entropy, [191 1M has the ability to monitor changes in high frequencies and a low capacity for monitoring phenomena at low frequencies. The achieved results in dead bean seeds with high and low water activity (Fig, 7) were similar to those found in living seeds reaffirming that even in high-frequencies the water has influence, and in this case, strongly linked to intense evaporation as observed in the graphical analysis. Fig. 8 also reinforces the hypothesis of the biological activity

influence throughout the speckle frequency in the seeds. However, it is ctear that to carry out separated analysis of biological activity in seeds from the water activity it is necessary to avoid the initial phase of intense evaporation even when carrying out the filtering. The influence of water, tear in that case, was also observed in a study to analyze the ocular microtremor by speckle approach [26]. In the corn seed, the most intense evaporation occurred at the crack can be linked to the intermediate bands helping future work, since it can be labeled as a signature of the evaporation of the water. Does the evaporation water cause biospeckle activity in that band of frequency in att the cases?

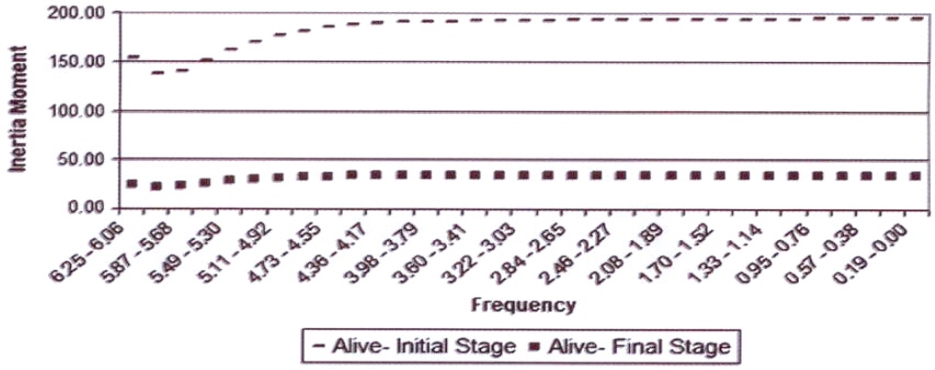

Figura 6 Behavior of the Inertia Moment in dead seeds with high and low water activity

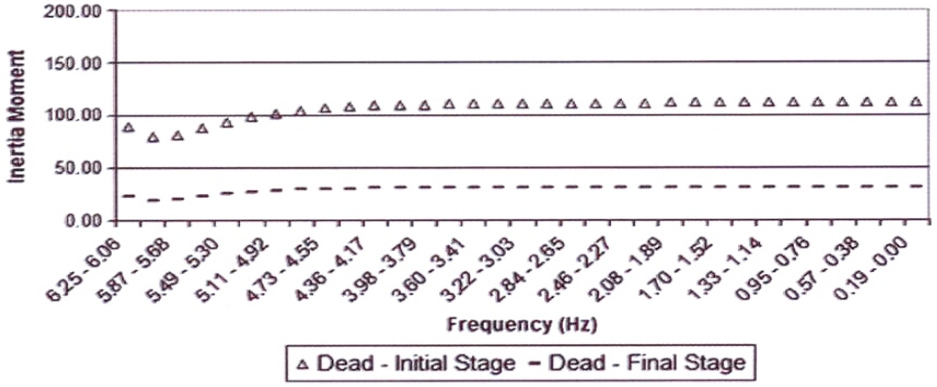

Figura 7 Behavior of the Inertia Moment in dead seeds with high and low water activity

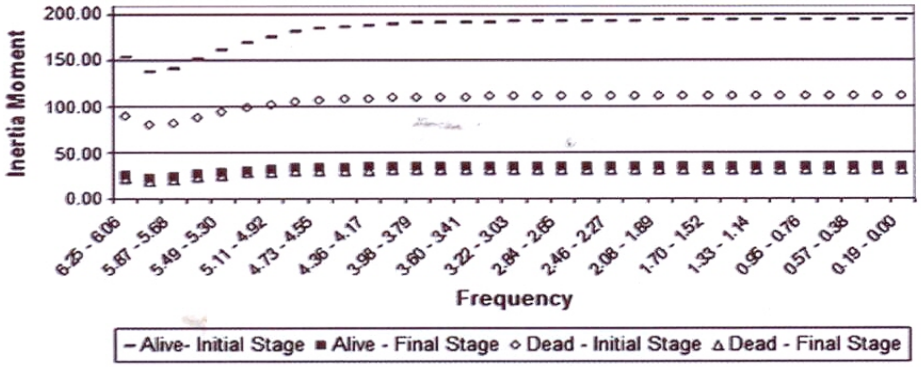

Figura 8 Behavior of the Inertia Moment in live and dead seeds with high and low water activity

5 Conclusions

This work presented steps to achieve actual isolation of biological phenomena by means of spectral approaches associating them to graphical and numerical routine methods. The observation of water activity in dilferent spectral ranges. and the evaluation of routine methods. presented novel information of the effort related to the separation of the phenomena responsible for the biospeckle patterns.

Acknowledgements

Special thanks to Federal University ofLavras. to FAPEMIG. to CNPq and to Finep.

REFERENCES

(1) H. Rabal, R.A Braga, Oynamic laser Speckle and Applications. CRC Press. New York.2008.

(2) G.F. Rabelo, R.A Braga. Rev. Bras. Eng. Agric. Ambient 09 (2005) 570.

(3) R.A. Braga Jr .• I.M. OalFabbro. F.M. Borem. G.F. Rabelo. R. Arizaga, H.J. Rabal. M. Trivi, Biosyst. Eng. 86 (2003) 287.

(4) R.A. Braga Jr .• G.F. Rabelo. LR. Granato. E.F. Santos. J.C Machado. R. Arizaga. HJ.
Rabal, M. Trivi. Biosyst, Eng. 86 (2005) 465.

(5) J.L Botega. RA. Braga. Rev. Bras. Eng, Agric. Ambient 13 (2009) 483.

(6) R.A. Braga. L Oupuy. Eur. Biophys. J. 38 (2009) 679.

(7) P.H. Carvalho. J.B. Barrete, R.A. Braga jr .. G.F. Rabelo. Biosyst, Eng. 102 (2009) 31.

(8) M.R. Trivi, in: H.J. Rabal, R.A Braga (Eds.). Dynamic Laser Speckle and Applications. CRC. 2008. p. 21.

(9) R.A. Braga. G.F. Rabelo. J.B. Barrete, F.M. Borem. J. Pereira. M. Muramatsu. I.M.O.
Fabbro, in: H.J. Rabal. R.A. Braga (Eds.). Oynamic laser Speckle and Applícations, CRC. 2008. p. 181.

(10) RA. Braga, G'w. Horgan. A.M. Enes. O. Miron. G.F. Rabelo. J.B. Barrete, Comput Electron. Agric. 58 (2007) 123.

(11) J.O. Briers. Opt, Commun. 13 (1975) 324.

(12) A.F. Fercher. J.O. Briers. Opt, Commun. 37 (1981) 326.

(13) P.li. S. Ni. L Zhang, S. Zeng, Q, tuo, Opt.Lert, 31 (2006) 1824.

(14) A. Daí Pra. I. Passoni. H.J. Rabal. Signal Processo 89 (2009) 266.

(15) I.L Sendra. R. Arizaga, H. Rabal. M. Trivi. Opt.l.ett. 30 (2005) 1641.

(16) M.F. limia. A.M. Núfrez, H. Rabal, M. Trívi, Appl. Opt, 32 (2002) 6745.

(17) I. Passoni. A. Dai Pra. H.J. Rabal. M. Trivi. R. Arizaga. Opt, Commun. 246 (2005) 219.

(18) R.A. Braga Jr .• W.S. da Silva. T. Sáfadi, CM.B. Nobre. Opt Commun. 281 (2008) 2443.

(19) C.M.B. Nobre. R.A. BragaJr .. A.G. Costa. R.R. Cardoso. W.S. da Silva. T. Sáfadi. Opt,
Commun. 282 (2009) 2236.

(20) A. OellAquila. Agron. Sustainable Oev. 29 (2009) 213.

(21) H. Fujii, T. Asakura. opr. l.ett. 10 (1985) 104.

(22) R. Arizaga. N. Cap, H.J. Rabal, M. Trivi, Opt, Eng. 41 (2002) 287.

(23) A. Oulamara, G. Tribillon.], Duvernoy.} Mod. Opt, 36 (1989) 165.

(24) Z. xu, c.joenatnan, B.M. Khorana. Opt, Eng. 34 (1995) 1487.

(25) R. Arizaga, M. Trivi, H. Rabal, Opt, taser Technol. 34 (1999) 1487.

(26) M. Alkalbani. E. Mihaylova. N. Collins, V. Toal. Proc. SPIE 7176 (2009) 717606.

ARTIGO 2 Biospeckle numerical values over spectral maps

R. A. Braga* [1], R. R. Cardoso [1], P.S. Bezerra [2], F. Wouters [2], G.R. Sampaio [2], M.S. Varaschin [2]
[1] Engineering Department, Federal University of Lavras UFLA, CP 3037 Lavras MG Brazil, robbraga@deg.ufla.br * Corresponding author
[2] Veterinary Medicine Department, Federal University of Lavras UFLA, CP 3037 Lavras MG Brazil, bezerraj@dmv.ufla.br

Esse artigo está em fase de submissão para o periódico Optics. O artigo está no formato em que foi submetido. A submissão foi feita pelo sistema de editorial da *Elsevier*, e o número de submissão é SM-1826. O processo de análise fruto do trabalho deste artigo gerou uma patente intitulada "BIOSPECKLE LASER COMO IDENTIFICADOR DE TECIDOS CANCERÍGENOS" com o número de protocolo 014110002539 junto ao INPI.

ABSTRACT

The image analysis presents itself as a powerful instrument applied to many sort of biological phenomena monitoring. The development of many optical approaches to carry out a feasible image assembling and analysis to different demands has been the main effort in this application area. A consequence of that effort is the adoption of the biospeckle laser technique as a potential alternative to pursue the optical metrology. Particularly, the monitoring of the biological activity under the laser illumination presents as a reliable tool to many applications in many areas, such as to identify the changes in the micro-blood flow in animal tissues, or even to monitor the vegetal and the animal tissues and their metabolism. However, one limitation of biospeckle is the access of graphical maps of activity with any numerical information linked to them. This work had the objective to present a protocol to separate different tissues in the same material by means of the frequency signature, and by means of the association of graphical and numerical results from the biospeckle laser images. In order to confirm the efficiency of the proposed protocol we applied it to separate embryo and endosperm in maize seed and as well as to separate tumour cells and normal tissues in animals. The results showed the feasibility of the approach proposed offering results with graphical maps associated to numerical information.

Keywords: Dynamic speckle. Frequency. Graphical and numerical analysis. Neoplasm. Seeds.

1 INTRODUCTION

The application of dynamic laser speckle, or biospeckle laser BSL, in many areas of knowledge created naturally new demands of research and developments (BRAGA et al., 2003; BRAGA et al., 2005; BRAGA et al., 2008; CARVALHO et al., 2009), but always carrying out the results with the separation of the graphical to the numerical approaches. In medicine the adoption of biospeckle laser has been widely used where a capillary blood flow in the human skin is present (BRIERS, 1975; BRIERS, 1993; FUJII, 1985), every time separating the graphical to the numerical approaches. Many applications in particular linked to the Doppler perfusion phenomenon and as well as to contrast technique were registered using graphical approaches (DUNN et al., 2003; RAJAN et al., 2006; SEROV; LASSER, 2005; TEARNEY; BOUMA, 2002). Despite the growing usage of dynamic laser speckle in blow flow phenomena, the use of biospeckle laser in tissues without a well defined flow was considered a more complex approach (ZHAO et al., 2002). The development of technologies associated with the dynamic laser speckle has offered new alternatives to access the sensitive activities in animal and vegetal tissues (BRAGA et al., 2008), in particular in those with a non-defined flux (AL-KALBANI et al., 2009) the ocular microtremor was evaluated.

The research of cancer identification, in turn, demands huge and permanent efforts to scientists such as to study the metastases (ZHDANOV, 2008). The optical techniques are an actual alternative to achieve the diagnosis of tumours which are also known as optical biopsy (KURACHI et al., 2008; LEE et al., 2010). The use of biospeckle in cancer cell detection can be observed in the literature (ANGELSKY; USHENKO; USHENKO, 2005) where the biospeckle and the Stokes vectors were adopted to early diagnostics of connective tissues pre-cancer states. In addition, a way to detect malignant

melanoma by laser speckle and contrast technique with numerical output was proposed (LEE et al., 2010) but without the generation of activity maps associated to numerical values. It is observed as well that the effort to achieve the cancer cell identification was also proposed in the frequency domain, in particular using the hyperspectral imaging (BANNON, 2009). In turn, the frequency domain has been one of the alternatives to achieve and enhance areas of different activities using biospeckle (RABAL et al., 2008). Differentiation of a low activity area inside the same tissue with high activity, like damage or fungi in seeds, is one challenge for the researchers. The study of seeds analysis in frequency domain in order to overcome the difficulty to isolate low activity areas has been presented (BRAGA et al., 2007; CARDOSO et al., 2011; SENDRA et al., 2005; PASSONI et al., 2005) searching for spectral signatures for the phenomena linked to seed activity.

This work aimed to present an approach to obtain numerical values for biospeckle phenomena within graphical maps of activity by means of frequency domain to create signatures to different activities, in particular linked to different cancer and seed tissues.

2 MATERIAL AND METHODS

The methodology adopted to evaluate the cancer cell identification was based on an image approach, in particular, using the Fujii Method (FUJII, 1985) before and after the frequency decomposition (Equation 1).

$$Fujii(x,y) = \sum_{k=1}^{N} \left| \frac{I_k(x,y) - I_{k-1}(x,y)}{I_k(x,y) + I_{k-1}(x,y)} \right| \quad (1)$$

Where the processed image, Fujii(x,y), represents the differences between the image Ik and the image Ik-1 in each pixel (x and y).

The frequency decomposition was carried out by the wavelets transform which was applied to each pixel of the 128 images (640x486 pixels) for the cancer tissues and 64 images (256x490 pixels) for the seed images assembled in time, as presented in Equation 2 with the wavelets coefficients being represented by CWT(t, j), as a function of time (t) and scale (j), from the signal in time f(t) being convolved with the Wavelet mother Morlet (TORRENCE; COMPO, 1998).

$$CWT(t, j) = f(t) * W(j, t) \quad (2)$$

After the decomposition of each pixel in time, the reconstruction of the collection of images was based on 25 and 21 scales of frequencies for cancer and seed tissues respectively from the wavelets transform as presented in the Equation 3 (TORRENCE; COMPO, 1998). The number of frequency ranges varied in accordance to the number of images assembled (BRAGA et al., 2008).

$$f(t) = K\sum_{j} \Re\{W(j,t)\} \quad (3)$$

Where the scale (j) represents a range of frequencies and K represents a constant, and the $\Re$ representing the real portion of the signal.

Each reconstruction generated a collection of new 128 images for cancer tissues and 64images for seed tissue with just one range of frequencies defined by the scales. The processing of Fujii Method was then conducted to each collection of the frequency scales producing an overlook to all the frequency answer.

The collection of images in frequency bands was analysed by the Space Spectral Speckle Matrix (3S Matrix) approach (MARQUES; BRAGA; PEREIRA, 2010) in the data from lines manually depicted in the interfaces between the normal and the cancer tissues.

A numerical analysis was conducted associating to the graphics results. For this reason two homogeneous areas of 40x40 pixels were extracted from the regions of cancerous and healthy tissues in a dog and cat and as well in embryo and endosperm tissues in a maize seed. The original frames were divided in windows of 40x40 pixels covering the entire image and the Inertia Moment (ARIZAGA; TRIVI; RABAL, 1999) values were obtained using the centre line of each one of this sub-areas. The sub-areas size were chosen for being representative for the areas evaluated, for not demand high machine processing and for being multiple for total image sizes. The effect of reduction in the amount of data analysed in each window was neglected (BRAGA et al., 2007).

The risk to crop a window with some noise was overcome using an homogeneity test which was calculated using the variance coefficient between IM values from the window in interest and the windows in its vicinity (Figure 1). The IM value of window five (IM5) was compared to the neighbourhood

(IM2, IM4, IM6, and IM8) as presented in Equation 4.

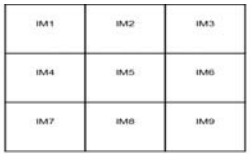

Figure 1 Window of interest (IM5) and its neighbourhood windows (IM2, IM4, IM6, and IM8) for homogeneity calculation

$$H_5 = 100.\frac{\sigma(IM_2, IM_4, IM_5, IM_6, IM_8)}{\mu(IM_2, IM_4, IM_5, IM_6, IM_8)} \quad (4)$$

Where σ(.) means the standard deviation of the IM values in the windows, and the μ(.) represents the mean values in the same windows. In the edges the homogeneity was calculated using only the windows present in the image.

One area with a low coefficient of variation within each type of tissue was chosen to represent the variation of the activity in 25 frequency ranges with the requirement that this area certainly is a representative portion of the studied tissue and that it does not have image defects such as saturation and dark areas.

The eligibility of the best window wasn't limited to the homogeneity test but also related to the quality of the image in point, with the analysis of histogram to search saturation or noises.

The numerical analysis was performed using the Inertia Moment methodology in these areas over the collection of images filtered in the frequency scales.

In all of these cases IM calculation was based on the the co-occurrence matrix from THSP (Time History Speckle Pattern) (ARIZAGA; TRIVI; RABAL, 1999) according to Equation 5.

$$IM = \sum_{i,j} M_{i,j}(i-j)^2 \quad (5)$$

Where i and j are the coordinates in the COM, which is the co-occurrence matrix built by the THSP of the speckle patterns. Equation 6 presents the normalization of the COM.

$$M_{ij} = \frac{COM_{ij}}{\sum_i N_{ij}} \quad (6)$$

Where N_{ij} is the number of time that the transitions i to j occurred in each line, in order to make the sum of values equal to one in each row of the matrix.

A relation between the values of IM found in each frequency scale for both tissues was made in order to find in which frequency bands there was a maximum differentiation. The biological materials chosen to be illuminated were neoplasic tissues from surgeries in a cat (skin) and in a dog (breast) and a maize seed which is a data routinely used in works related to the biospeckle studies. The maize seed had moisture over 20% of wet base and was cut in its middle before the illumination. The neoplasic tissues were from surgeries in a cat (skin) and in a dog (breast), and were analyzed before the histological exams. They were maintained cooled just after the surgeries and they were not fixed in phormaldehyde which is a routine step to implement histological exams. The samples were cut in pieces creating a flat surface with the neoplastic and the normal tissues naturally linked side by side. After the illumination, the neoplastic tissue were fixed in phormaldehyde 10%, and dehydrated through increasing concentrations of ehtyl alcohol, diaphanized in xylol and included in paraffin in order to be analyzed in histological exams. The cuts of 5µm were pigmented using Hematoxylin-Eosin (HE) staining protocol, and the neoplastic diagnosis were conducted in accordance to histological and to pathological

aspects (MEUTEN, 2002).The experimental configuration of the illumination can be seen in Figure 2, where the dynamic laser speckle approach adopted was the backscattering speckle.

A laser set of HeNe with 10mw, of 632nm, was opened and illuminated the sample directed by a mirror. The CCD camera and the computer were responsible for the assembling of the images with 256x490 pixels for the seed and 486x640 pixels for the animal tissues summing 64 and 128 frames for maize seeds and neoplastic tissues respectively, both in a rate of 0.08s.

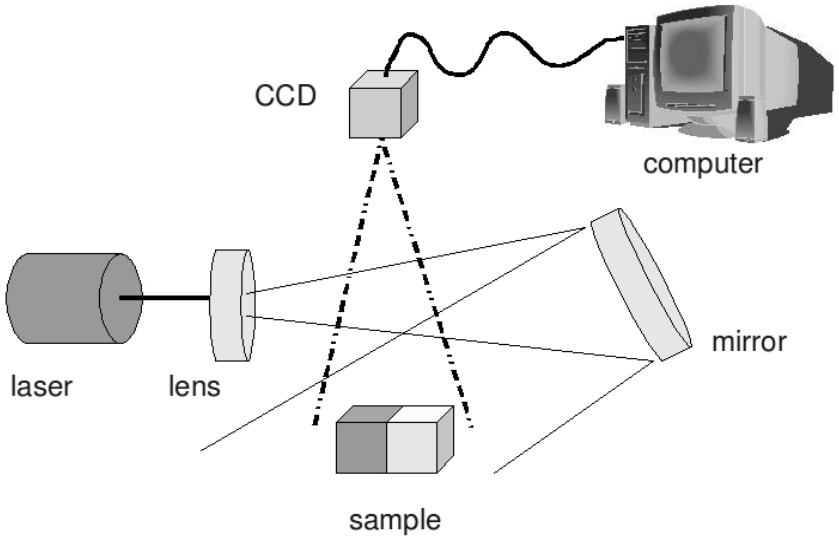

Figure 2 Backscattering experimental configuration of tissues illumination and image acquiring

3 RESULTS

3.1 In Maize Seed

The homogeneity variability in maize seeds using the Equation 4 is displayed in Figure 3. The areas chosen to represent the embryo and the endosperm are shown in Figure 4. In Figure 5 it is possible to see the Fujii result in background the homogenous windows selected in the embryo and in the endosperm to be analyzed.

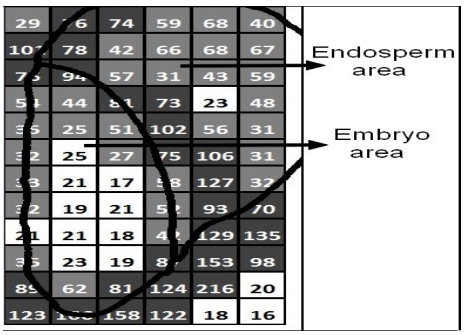

Figure 3 Homogeneity values distribution in maize seeds using the IM

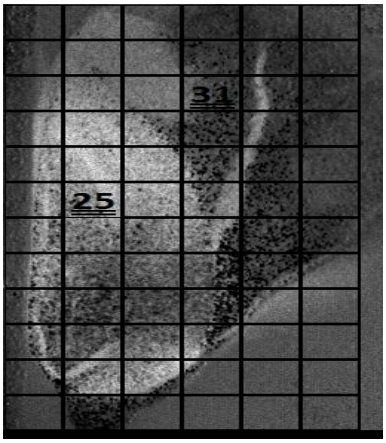

Figure 4 Extracted homogenous areas in Fujii treatment

The numerical information from the levels of activity within homogeneous portions of the endosperm and embryo tissues over all frequency bands are showed in Figure 4. It can be observed that the activity in embryo tissue is significantly higher than the activity in endosperm tissue upward 3.5 Hz. In Figure 6 it is presented the relations between the IM values over all the bands and frequencies of 5.36 to 6.25Hz were better to differentiations between the tissues. Also, in Figure 5, it is possible to observe that the endosperm presents higher activity than the embryo at frequencies bellow 0.89 Hz.

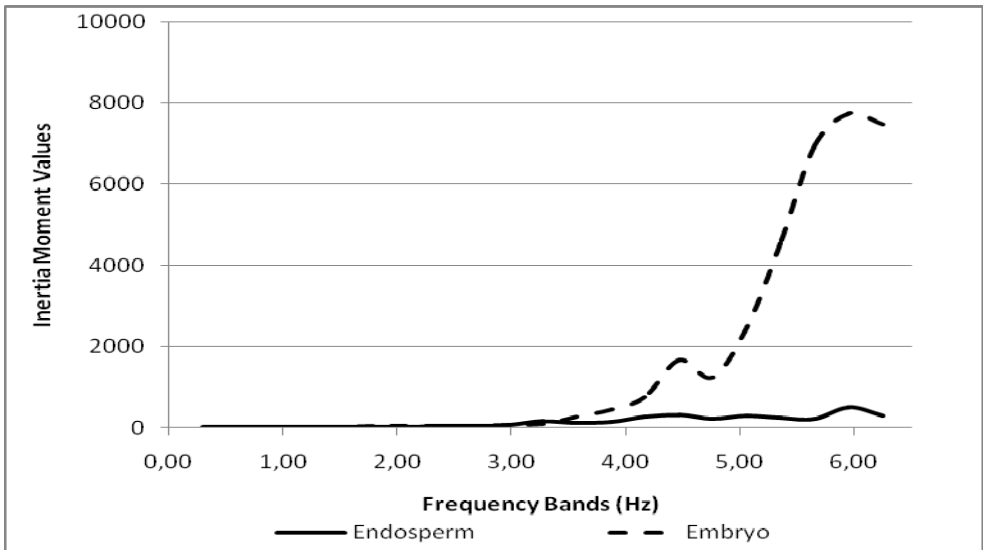

Figura 5 IM values over 21 frequency scales for endosperm and embryo in maize seed

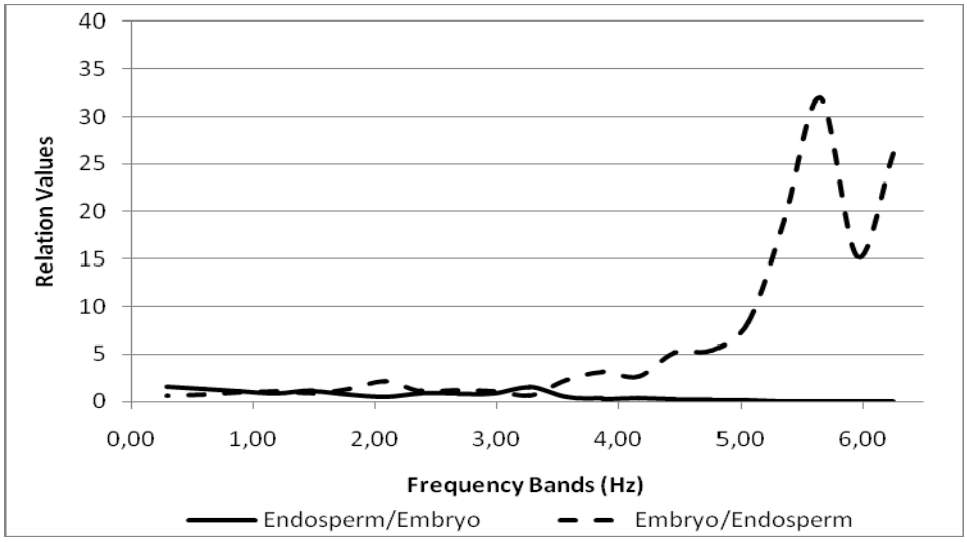

Figure 6 Relation between IM from different tissues in 21frequency scales

The numerical analysis in the maize seed improved and complemented the graphical analysis. In addition, the use of spectral bands improved even more the differentiation allowing a better use of frequency signatures (CARDOSO et al., 2011) of each tissue. Although this is a robust method, it is necessary to previously know the images or/and to properly make the image acquisition. The maize seed analysis was chosen because it is a good example about the quality of the images, and because it is well known in the literature. Therefore, the area analysed in the endosperm should avoid the crack area, and, in the embryo, the saturation in its middle distorted the actual results expected. For this reason it was chosen a different area in a homogeneous portion in the embryo as well.

3.2 In cancer cells

The neoplasic tissues were histologicaly classified as basosquamous carcinoma in the feline's skin and anaplastic mammary carcinoma in a female

canine. The anaplastic mammary carcinoma, besides its distinct cell origin, presented lower differentiation if compared to the basosquamous carcinoma . In turn, the anaplastic mammary carcinoma was plenty of fibrous stroma while it was rare in the basosquamous carcinoma, and in addition the anaplastic mammary carcinoma had areas of *inflammatory infiltrate* dominated by *neutrophils* which was either absent in the *basosquamous carcinoma.* In Figure 7 it is possible to observe the images from histological sections with the basophilic neoplastic tissues. In Figure 7a, the basosquamous carcinoma can be seen in dark, and a normal tissue in the right bottom of the image with light (eosinophlic), in a format of a tail. The anaplastic mammary carcinoma is observed in the Figure 7b in dark situated below and the normal tissue in light in the top of the image.

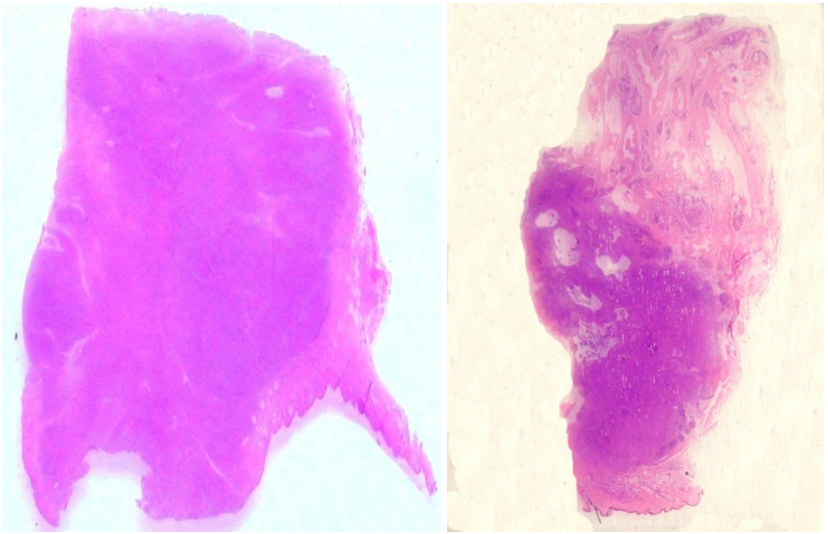

(a) (b)

Figure 7 Histological analysis of samples with (a) a skin cancer in dark connected to a thin normal tissue, and with (b) a breast cancer in dark connected to a normal tissue

The results related to the spectral bands of the samples are presented in Figure 8 and 9, where the images are pseudo-colored (or gray), with in the extremes the red color (light gray) meaning high activity and the blue color (dark gray) meaning low activity after Fujii process.

In Figures 8 and 9, the original Fujii process means that the method was carried out without any filtering, and the 25 images above the original one are related to the Fujii processing with each frequency band from 0 to 6.25 Hz. Each image is related to a range of 0.25 Hz and the number is related to the first frequency of the range.

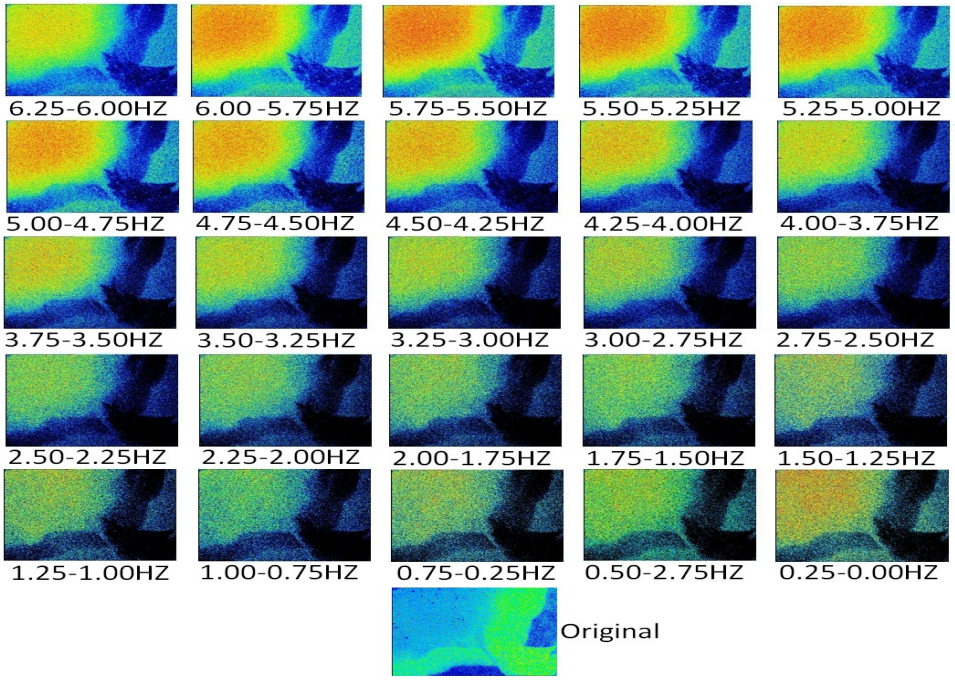

Figure 8 Spectral ranges of a basosquamous carcinoma under biospeckle analysis with the last image representing the original processing without filtering. The high activities are represented by red in pseudo-color or light gray, and the low activities are dark blue in pseudo-color or dark gray

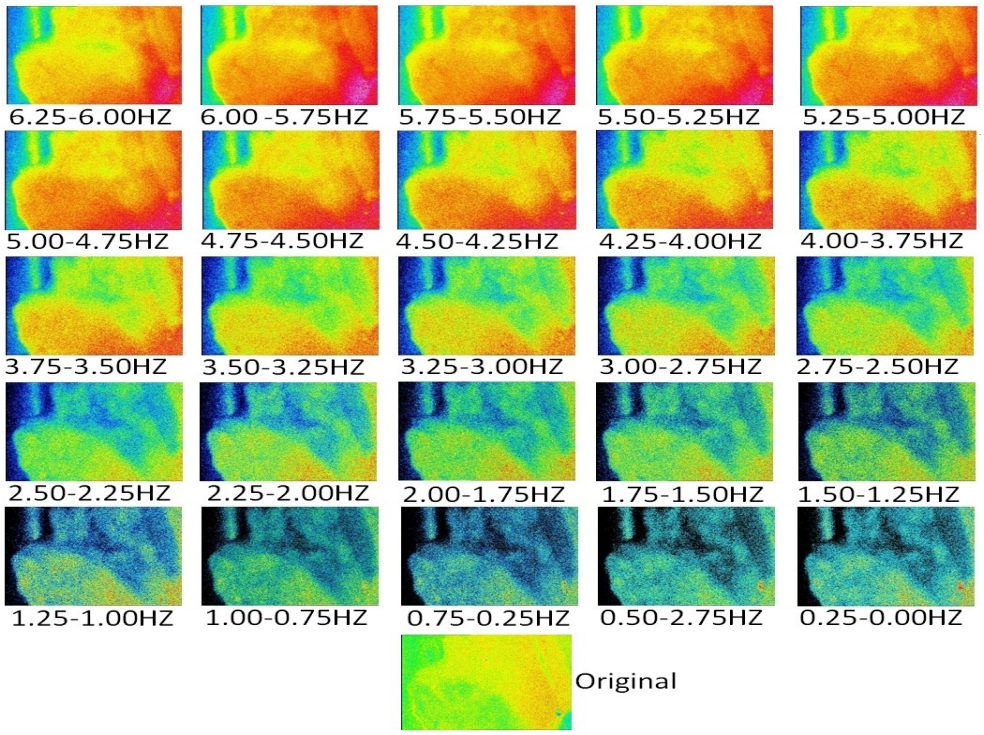

Figure 9 Spectral ranges of an anaplastic mammary carcinoma under biospeckle analysis with the last image representing the original processing without filtering. The high activities are represented by red in pseudo-color or light gray, and the low activities are dark blue in pseudo-color or dark gray

The Fujii processing in cat tissues presented any separation in the original routine, in turn the whole spectral bands made it possible to observe that the cancer cells were more active in the higher frequencies, while in the tail of the sample, where it was the normal tissue, the activity presented a low profile in all frequencies.

In Figure 9 it is possible to see the ability to separate the cancer tissue from the normal one using the original approach, otherwise, in spectral bands it

was assigned in what frequencies the neoplastic tissues were more active.

In Figure 10, the 3S Matrix is presented and, in particular in the Figure 10a, it is possible to see where are the values, used to construct the 3S in the basosquamous carcinoma. Similarly, Figure 11a presents the same information about the anaplastic mammary carcinoma.

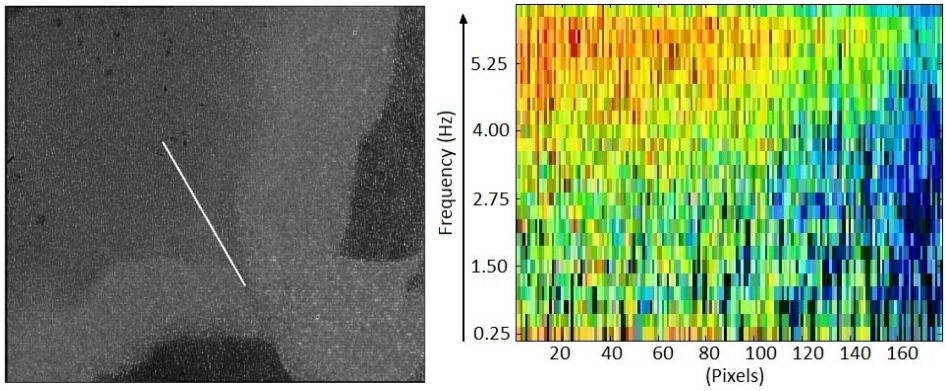

(a) (b)

Figure 10 Space-Spectral Speckle Matrix (3S) formation (a) with the line crop in the basosquamous carninoma and normal tissue, and (b) the 3S Matrix with the frequencies and the interface between the tissues

The information from the collection of all the 25 spectral ranges was therefore expressed in just one image, assigning a strip-line as reference. These lines were crop from the images in a same position and placed one over the other in the 3S Matrix. The x axis of the image is therefore related to the pixels of the strip-line and the values of the activity, assigned by the Fujii method and expressed in levels of gray, are addressed in axis y related to the 25 spectral bands.

In Figure 10b, still related to the basosquamous carcinoma, the 3S Matrix presents that the cancer cells had high activity (colour in red or bright gray) in the range of high frequencies as well as in the extreme low frequencies.

The same evaluation can be seen in the 3S Matrix of the anaplastic

mammary carcinoma with different behaviour in the range of frequencies activated by the cancer, in particular observed by the absence of expression of the cancer in the low frequencies (Figure 9).

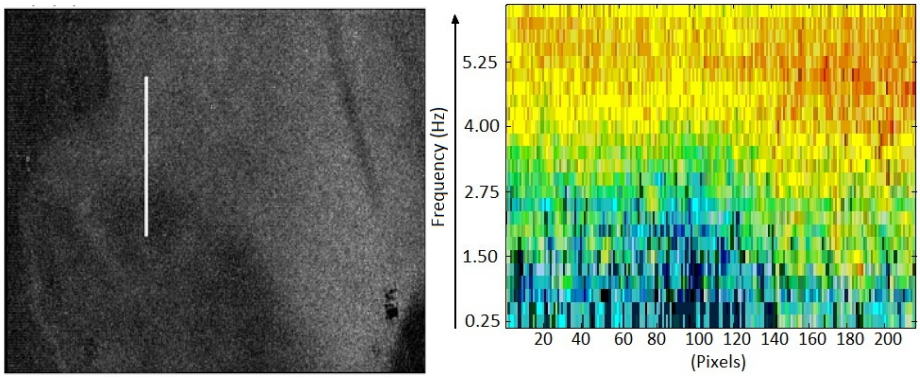

(a) (b)

Figure 11 Space-Spectral Speckle Matrix (3S) formation (a) using the line crop in the anaplastic mammary carninoma and normal tissue, and (b) the 3S Matrix with the frequencies and the interface between the tissues

Another observation obtained from the 3S Matrix from the both cancers are the clear definition of the transition between the normal and neoplastic tissues.

In turn, the information observed in the graphical analysis was improved by the numerical values of Inertia Moment [28]from the levels of activity within homogeneous portions of the different tissues. Figure 12 shows the homogeneity distribution in mammary carcinoma as well the areas chosen to represent cancer and healthy tissue. Figure 13 highlighted the homogenous areas to the two regions extracted from the biospeckle laser image analyzed by Fujii technique.

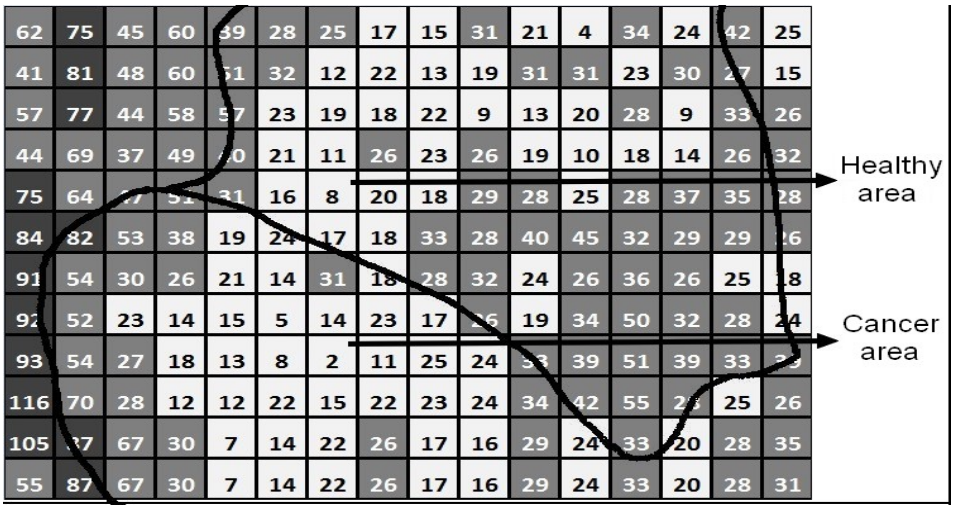

Figure 12 Homogeneity distribution in mammary carcinoma

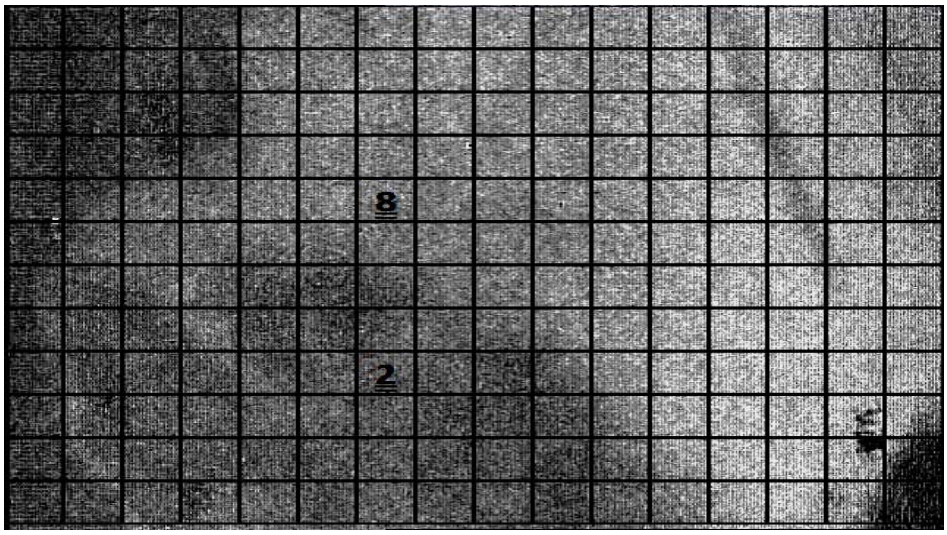

Figure 13 Extracted homogenous areas in Fujii treatment

In the selected areas showed in Figure 12, the IM was calculated in conventional way in the 25 frequency scales and it can be observed that the activity in cancerous tissues, in this stage, was always higher than the activity in

normal tissue (Figure 14). For this case, the commons bands frequencies for better differentiations (Figure 15) in IM value happens in scales 6 to 7 (5.00 to 4.50Hz) and in scales 11 and 12 (3.75 to 3.25 Hz).

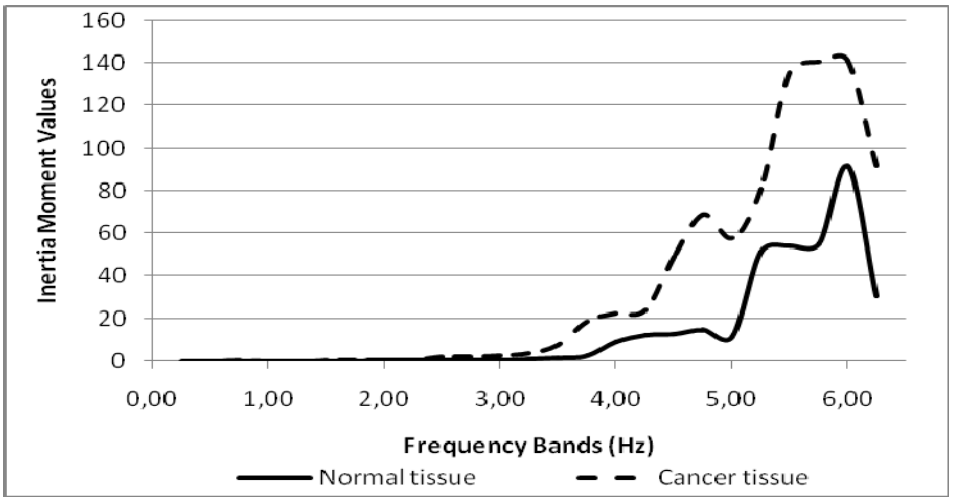

Figure 14 IM values over 25 frequency scales for mammary carcinoma and normal tissue

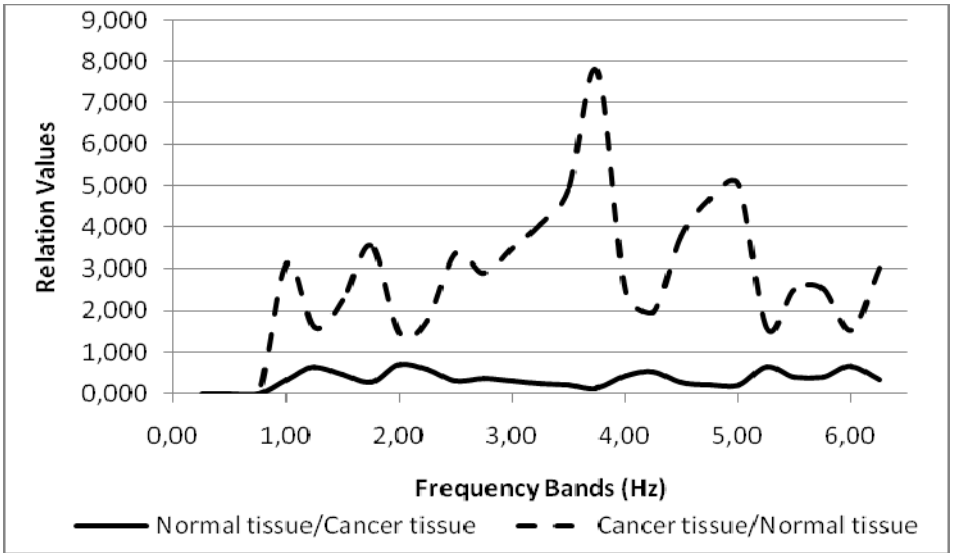

Figure 15 Relation between IM from different tissues in 25 frequency scales

Similarlly, Figure 16 shows homogeneity distribution and the homogeneous areas chosen to represent the basosquamous carcinoma and the normal tissue. Figure 17 shows these areas after Fujii analysis.

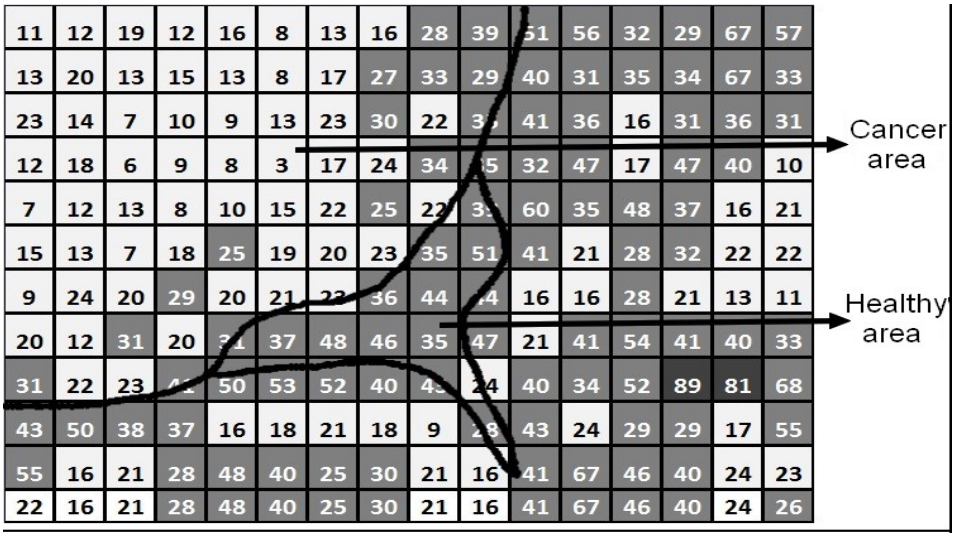

Figure 16 Homogeneity distribution in basosquamous carcinoma

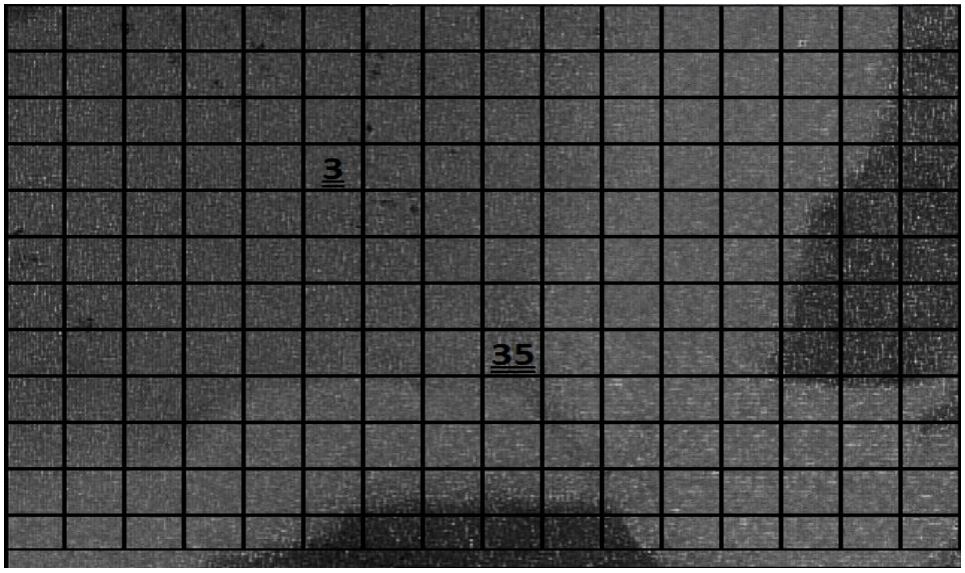

Figure 17 Extracted homogenous areas in Fujii treatment

Similarly to Figure 14 and 15, Figure 18 presents the results using the Inertia Moment in basosquamous carcinoma. As it happens with mammary it can be observed that the activity in this carcicoma is always higher than the activity in normal tissue. For this case, it was possible to get more bands with high differences between the tissues under laser illumination (Figure 19).

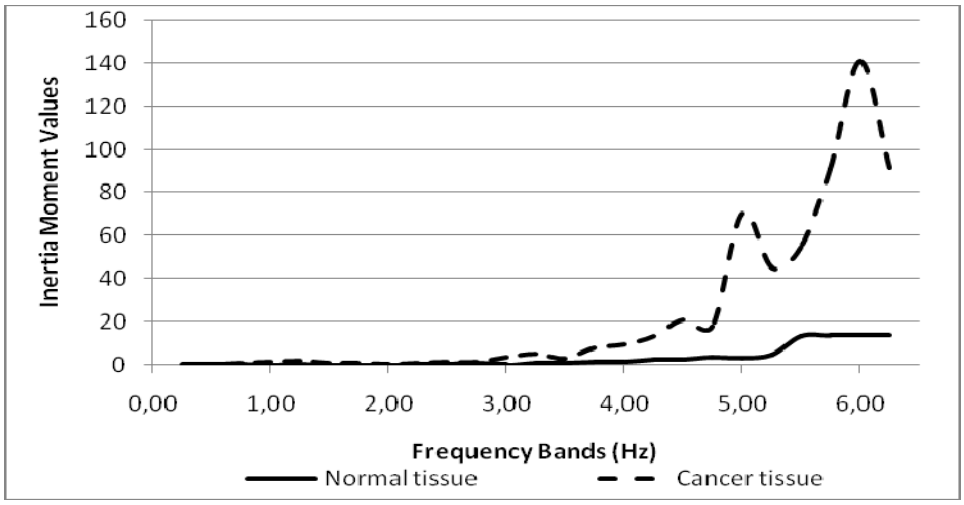

Figure 18 IM values over 25 frequency scales for basosquamous carcinoma and normal tissue

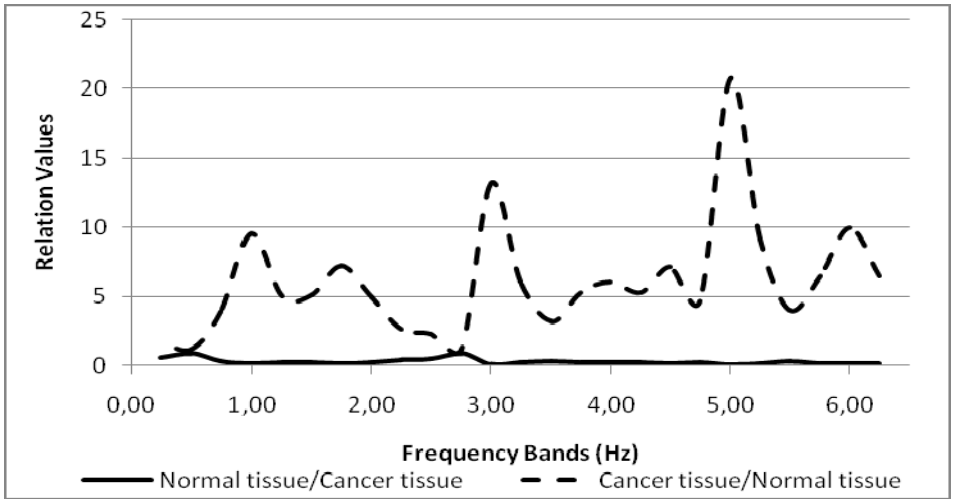

Figure 19 Relation between IM from different tissues in 25 frequency scales

4 CONCLUSIONS

In this work an alternative protocol to assess the information from the biospeckle phenomena was presented by the association of graphical and numerical outputs under the spectral domain. The maps of activity presented in the graphical results associated to the numerical values were tested in a well known sample, the differentiation of the embryo and the endosperm in a corn seed, and the differentiation of the normal and neoplastic in animal tissues.

Acknowledgements

This work was supported by UFLA, CNPq, Fapemig, Capes and Finep.

REFERENCES

AL-KALBANI, M. et al. Ocular microtremor laser speckle metrology. **Proceedings of SPIE**, Bellingham, v. 7176, p. 606, 2009.

ANGELSKY, O. V.; USHENKO, A. G.; USHENKO, Y. G. Stokes Polarimetry of Biospeckle Tissues Images in Pre-Clinic Diagnostics of Their Pre-Cancer States. **Journal of Holography and Speckle**, Nashville, v. 2, p. 26-33, 2005.

ARIZAGA, R.; TRIVI, M.; RABAL, H. J. Speckle time evolution characterization by the co-occurrence matrix analysis. **Optics & Laser Technology**, Benevento, v. 31, p. 163-169, 1999.

BANNON, D. Hyperspectral imaging. **Cubes and slices Nature photonics**, London, v. 3, p. 627-629, 2009.

BRAGA, R. A. et al. Applications in biological samples. In: Rabal, H. J.; Braga, R.A. (Ed.). **Dynamic laser speckle and applications.** Boca Raton: CRC, 2008. p. 181-231.

BRAGA, R. A. et al. Assessment of Seed Viability by Laser SpeckleTechniques. **Biosystems Engineering**, London, v. 86, p. 287-294, 2003.

BRAGA, R. A. et al. Biological feature isolation by wavelets in biospeckle laser images. **Computers and Electronics in Agriculture**, Amsterdam, v. 58, p. 123-132, 2007.

BRAGA, R. A. et al. Detection of Fungi in Beans by the Laser Biospeckle Technique. **Journal of Agricultural Engineering Research,** Edinburgh, v. 91, p. 465-469, 2005.

BRAGA, R. A. et al. Live biospeckle laser imaging of root tissues**.** **European Biophysics Journal**, Berlin, v. 38, n. 5, p. 679-686, 2009.

BRAGA, R. A. et al. Reliability of biospeckle image analysis. **Optics and Lasers in Engineering**, Lausanne, v. 45, p. 390-395, 2007.

BRIERS, J. D. Speckle fluctuations and biomedical optics: implications and applications. **Optics Communications**, Sydney, v. 32, p. 277-283, 1995.

BRIERS, J. D. Wavelength dependence of intensity fluctuations in laser speckle patterns form biological specimens. **Optics Communications**, Sydney, v. 13, p. 324-326, 1975.

CARDOSO, R. R. et al. Frequency signature of water activity by biospeckle laser. **Optics Communications**, Sydney, v. 285, p. 2131-2136, 2011.

CARVALHO, P. H. A. et al. Motility parameters assessment of bovine frozen semen by biospeckle laser (BSL) system. **Biosystems Engineering**, London, v. 102, p. 31-35, 2009.

DUNN, A. K. et al. Simultaneous imaging of total cerebral hemoglobin concentration, oxygenation, and blood flow during functional activation. **Optics Letters**, Washington, v. 28, p. 28-30, 2003.

FUJII, A. H. Blood-flow observed by time-varying laser speckle. **Optics Letters**, Washington, v. 10, n. 3, p. 104-106, 1985.

KURACHI, J. D. et al. **Detecção óptica no diagnóstico**. São Paulo: Livraria da Física , 2008. p. 81-96.

LEE, T. K. et al. Towards automatic detection of malignant melanoma by laser speckle. **Proceedings of SPIE**, Bellingham, v. 7387, p. 73871, 2010.

MARQUES, J. J. K.; BRAGA, R. A.; PEREIRA, J. Areas of activity in biofilms trough the biospeckle and spectral domain. **Proceedings of SPIE**, Bellingham, v. 7387, p. 73871A, 2010.

MEUTEN, D. J. **Tumors in domestic animals.** 4th ed. Iowa: Blackwell, 2002. 788 p.

PASSONI, A. et al. Dynamic speckle processing using wavelets based entropy. **Optics Communications**, Sydney, v . 246, p. 219-228, 2005.

RABAL, H. J. et al. **Dynamic laser speckle and applications.** Boca Raton: CRC, 2008. p. 251.

RAJAN, V. et al. Speckles in laser Doppler perfusion imaging. **Optics Letters,** Washington, v. 31, n. 4, p. 468-470, 2006.

SENDRA, G. H. et al. Decomposition of biospeckle images in temporary spectral bands. **Optics Letters**, Washington, n. 30, n. 13, p.1641-1643, 2005.

SEROV, A.; LASSER, T. High-speed laser Doppler perfusion imaging using an integrating CMOS image sensor. **Optics Express**, Washington, v. 13, p. 6416-6428, 2005.

TEARNEY, G. J.; BOUMA, B. E. Atherosclerotic plaque characterization by spatial and temporal speckle pattern analysis. **Optics Letters**, Washington, v. 27 p. 533-535, 2002.

TORRENCE, C.; COMPO, G. P. A practical guide to wavelets analysis. **Bulletin of the American Meteorological Society,** Washington, v. 79, p. 61–78, 1998.

ZHAO, Y. et al. Point-wise and whole-field laser speckle intensity fluctuation applied to botanical specimen. **Optics and Lasers in Engineering**, Lausanne, v. 28, p. 443-456, 1997.

ZHDANOV, V. Stochastic model of the formation of cancer metastases via cancer stem cells. **European Biophysics Journal**, Berlin, v. 37, p. 1329-1334, 2008.

ARTIGO 3 Improvements on dynamic speckle laser analysis

Esse artigo está em fase de revisão e será submetido à *Signal Processing*.

Improvements on dynamic speckle analysis techniques

R. R. Cardoso [1], R. A. Braga* [1]

[1] Department of Engineering, Federal University of Lavras UFLA, CP 3037 Lavras MG Brazil, robbraga@deg.ufla.br * Corresponding author

ABSTRACT

Biospeckle or dynamic laser speckle is a phenomenon developed when a dynamic process occurs in a material under laser illumination and this phenomenon contains considerable information related to both biological and non-biological activity of the material under study. Analysis of dynamic speckle laser is performed with techniques of digital image processing and statistical analysis. As a non-invasive, non-destructive and low cost technique, biospeckle laser (BSL) has been an outstanding tool for monitoring biological properties. Thus, its application in optical instrumentation has grown over the years, especially in the areas of biology, medicine and agriculture. However, this analysis has been a challenge for specialists due to the complex interaction between light and material expressed, for instance, by the high sensitivity of the biospeckle laser (BSL) technique, the variability of biological material combined with the large number of variables involved in speckle pattern formation beginning with the setup of the experimental configuration. This study aimed to improve the BSL techniques presenting alternatives to numerical and graphical approaches, in order to enhance the robustness, to reduce the subjectiveness and the dependence of the human being expertise during the setup. The work was based on the creation of requirements to achieve the best speckle patterns such as evaluating the saturation, the homogeneity and the contrast of the grains. The analysis of the numerical methods was based on the improvements of a traditional method robustness, and in turn it was addressed an alternative approach to enhance the graphical image. The results presented the importance of the primary steps to achieve quality in the speckle pattern under analysis, and as well the relevance of robustness improvements in the numerical Inertia Moment method. The alternative to graphical method based on standard deviation presented a better result if compared to the traditional ones.

1 INTRODUCTION

Dynamic laser speckle is an optical phenomenon formed when an object in dynamic activity is illuminated by light with high coherence, for instance of laser. The activity of biological materials, such as growth and cell division, cytoplasmic movement and biochemical reactions, besides water-related activities, changes the microscopic structure of the material illuminated by a laser source (BRAGA et al., 2009). Such changes make the interference pattern formed by scattering light on objects shift over time, giving rise to dynamic laser speckle.

Optical instrumentation is advantageous as it is a non-invasive, non-destructive and low cost technique (TCHVIALEVA et al., 2010) and has been an outstanding tool for assessing and monitoring biological properties (BRIERS, 1975; RABAL; BRAGA, 2008). Thus, BSL application has grown in optical instrumentation over the years, especially in the areas of biology [4], medicine (GONIK; MISHIN; ZIMNYAKOV, 2002) and agriculture (CARVALHO et al., 2009; PAJUELO et al., 2003).

Dynamic laser speckle analysis uses techniques of digital image processing and statistical analysis, which can be divided into two basic types: graphical analysis resulting in maps showing spatial variability of BSL activity level, such as the Fujii Method (FUJII et al., 2009), and Generalised Differences (ARIZAGA; CAP; RABAL, 1985) or numerical analysis, which results in quantification of activity of the biological or non-biological material, as the Inertia Moment (IM) technique (ARIZAGA; TRIVI; RABAL, 1999).

The complexity of the phenomenon the great number of variables involved in dynamic speckle formation, especially in biological materials, have demanded development of safer, more robust methods. In addition, the experimental configuration setup which is essential for achieve quality and

consequently consistency in the analysis, is usually based on researchers experience which amplify subjectivism in BSL analysis. The data processing, including the noise in speckle imaging has been studied and evaluate in order to enhance reliability in BSL analysis (BRAGA et al., 2008; SKIPETROV et al., 2010).

There are works, presenting solutions and improvements on classic techniques for BSL analysis, for example, the IM calculation has been modify (BRAGA et al., 2011) in order to improve the measurement of activity at low frequencies (NOBRE et al., 2009). In these sense, numerical techniques has been compared and evaluate according to coherence, consistency, spectral range and differentiation between different samples (ZDUNEK et al., 2007). In addition, there are sophisticated techniques for graphical output in BSL analysis (BRAGA et al., 2007; DAI PRA; PASSONI; RABAL, 2009) which enhances and improves conventional graphical outputs which differentiates BSL areas in frequency and even by creation of spectral signatures (CARDOSO et al., 2011) for some phenomena. However in order to fully validate the technique of dynamic speckle as an optical instrument, demand for new research is still high. There still is a need for methodiser and create new protocols for BSL analysis techniques, such as adoption protocol for avoid subjectivism in illumination phase, reduces high dispersion between samples in numerical analysis, capture quick activity changes in shorter times in BSL and create a more quickly and better quality graphical technique.

Therefore, this study aimed to develop and refine methodologies for the BSL analysis and create protocols for different types of analysis. In particular, we present a protocol to obtain requirements before the main analysis, in an attempt to eliminate image quality based on subjectivism or research experience. We also present improvements in IM method, which gives reliability advantages such as reduction of the coefficient variation between samples besides the

continuous IM, which has the ability to continuously monitoring the activity level fluctuation in a sample over time. In addition, we present a new graphical method with great potential when compared to classic techniques, due to better quality on final image and processing time.

2 MATERIAL AND METHODS

2.1 Introduction

The modifications of classic techniques and new approaches for BSL analysis were processed at three levels. First of all, the BSL image quality during illumination phase was evaluated by means of assessment of saturation and dark areas, speckle pattern formation and image homogeneity.

In second place, the IM calculation was modified in two ways: changing Occurrence matrix normalization and reducing temporal information.

Finally, a graphical tool based on standard deviation it is presented.

2.2 BSL image quality

The methodology used to evaluate the image quality resulting from experimental configuration and material properties was based on spatial variation of saturation and dark areas, contrast level and activity homogeneity.

Each image in a set of images was divided in small areas with 40x40 (1600 points) pixels in order to assess saturation and dark areas. For all frames, the grey level was observed in the pixels inside each area. Areas were classified in three kinds: saturation, normal or dark area. The methodology adopted to classify the areas for 8 bit imagery is presented in Equation 1.

$$Classifled\ Area = \begin{cases} Occ_{px=255} > 1600.N.0.05 \rightarrow Saturated\ area \\ Occ_{px=0} < 1600.N.0.05 \rightarrow Dark\ area \\ Occ_{0<px<255} \geq 1600.N.0.95 \rightarrow Normal\ area \end{cases} \quad (1)$$

Where N is the number of images, and the classification depends on

pixel grey level occurrences (Occ) for each area.

Contrast level is acquired for each 40x40 pixel area. This measure gives an idea about grain formation in speckle pattern (RABAL; BRAGA, 2008). Equation 2 shows the contrast calculation.

$$C = \frac{\sigma}{\langle I \rangle} \quad (2)$$

Where $\langle I \rangle$ and σ represent the average and the standard deviation of grey level intensity, respectively, for each study area. As calculation includes all frames, the contrast value for each area was adopted as the mean contrast for every frame.

Similarly, the homogeneity was evaluated by means of activity spatial distribution using Inertia Moment (IM) method. It was obtained the IM technique for each sub-area, considering that reduction in spatial information does not affect IM activity measuring (NOBRE et al., 2009). This process results in a new spatial reduced matrix which gives numerical information about the distribution of spatial activity. Homogeneity is calculated over this matrix, by comparing the similarity between each IM and its vicinity through the coefficient of variation. For each area the vicinity was defined as the four nearest IM values to the left, right, up and down. The choice of better threshold to homogeneity is still dependent of human evaluation.

2.3 Inertia moment improvements

The IM method (ARIZAGA; TRIVI; RABAL, 1999) is based on the co-occurrence matrix (COM) (HARALICK; SHANMUGAN; DINSTEIN, 1973) of the time history speckle pattern (THSP). Equation 3 shows the IM calculation.

$$IM = \sum_{i,j} M_{ij} (i - j)^2 \quad (3)$$

Where M is the normalised value for COM in coordinates i and j. The conventional normalisation proposed (ARIZAGA; TRIVI; RABAL, 1999) is shown in Equation 4.

$$M_{ij} = \frac{COM_{ij}}{\sum_i COM_{ij}} \quad (4)$$

Where COM_{ij} is the COM value in row i and column j. Thus, normalisation makes the sum of values in each row of the COM equal to one. A new normalisation is proposed, which has the entire COM equal to one according to Equation 5.

$$M'_{ij} = \frac{COM_{ij}}{\sum_{i,j} COM_{ij}} \quad (5)$$

The IM methods with different normalisations were tested in repeatability and variance between samples of biological material. In addition, the activity measuring ability was tested in both methods, reducing spatial and temporal information in homogeneous samples.

The typical THSP has the entire time information of an image group. Thus, the activity changes in the material over time, which the image group represents, are quantified by one number. The continuous IM was calculated by using a floating window which reduces time information to obtain the activity variability in time, represented by all frames in the image group. If this window has width equals to the number of images, the continuous IM has the same value of classic IM. Equation 6 compares the classic IM with continuous IM method.

$$THSP_{time \to 1\ to\ N} \to IM$$
$$THSP_{time} \to \sum_{i=1}^{N/W} [i.W - (W-1)\ to\ i.W] \to Continuous\ IM \quad (6)$$

Where W is the width of the time-window used. Continuous IM was calculated by varying time-window, generating N/W numeric results. The Continuous IM method was used to obtain the awakening moment of a dormant seed. The image group was composed by 185 frames with 480x640 pixels in a rate of 0.08 seconds. For this case, the results obtained by using Continuous IM were compared to classic IM method.

2.4 Graphical technique

The graphical technique was based on standard deviation of each pixel over time. Equation 7 shows this concept.

$$sd^2(x,y) = \sum_{i=1}^{N} \frac{[P(x,y,i) - \mu(x,y,i)]^2}{N} \quad (7)$$

Where each intensity level P at the coordinates (x,y) for each frame i are subtracted by the mean intensity for the same coordinates of frame 1 to N followed by division by N. The numerical outputs are normalised according to Equation 8.

$$SD_{i,j} = \left(\frac{sd_{i,j}}{\max(sd_{i,j})}\right).255 \quad (8)$$

This graphical technique was compared to Fujii and Generalized Differences (GD) methods in processing time and final image quality issues, using live root tissue by BSL images [1].

3 RESULTS AND DISCUSSION

3.1 Requirements for BSL image quality

Saturated or dark areas in BSL images could create false activity impressions or mask real activity occurring in the material under study. Not only the knowledge about the existence of this image defects is significant, but also the location of saturation or dark area is important in many experiments with dynamic speckle due to use of contrasting background, usually white or black, and other variables involved in illumination experiments.

The map of activity of a maize seed generated by GD method in Figure 1a shows a lack of activity in the middle region of the embryo. This occurs due to mask effect caused by saturation in the area. Figure 1b shows the histogram of a 40x40 pixel area positioned in saturated and normal area of a participant image.

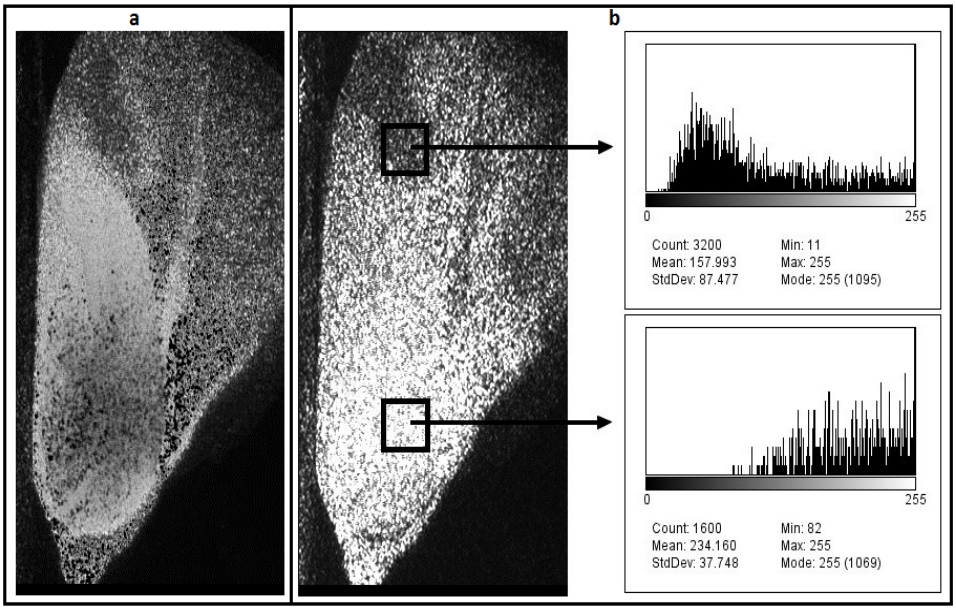

Figure 1 Saturation observed in maize seed

Figure 2 presents a graphic result using the methodology for areas classified according to pixel intensity. It can be observed that saturated areas could be identified for this image group. All participant frames are included in this classification, which shows that the 255 occurrence is high in a large part of the BSL image. In the centre of the embryo area, the 255 occurrence becomes higher than 60%. That was the dark area classified for this image group. This classification could be improved by using thresholds defined by fuzzy method.

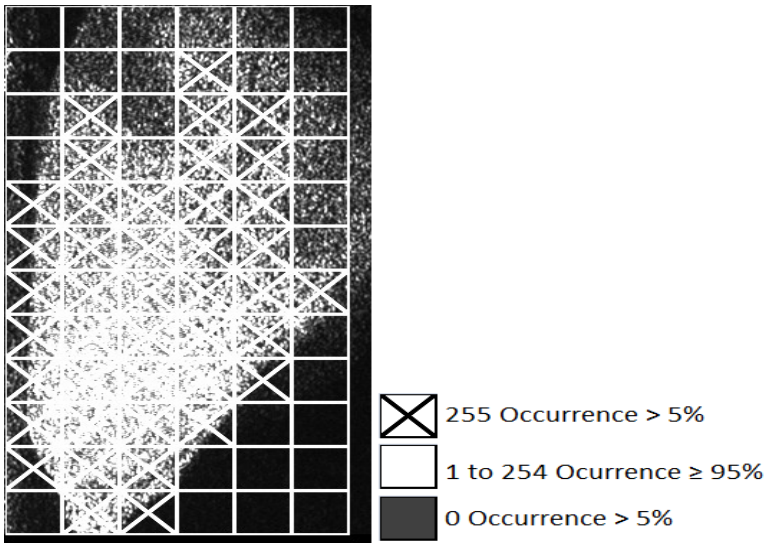

Figure 2 Percentage occurrence in maize seed

The well-formed speckle pattern has the contrast value near 1. When there is no speckle pattern formation the contrast value is close to zero, thus the contrast value could vary from zero to one according to grain formation, giving an idea of image quality of the speckle pattern. Results from an experiment of drying paint on a coin surface are shown in Figure 3. Figure 3a presents a numerical analysis using IM method to quantify the activity of ink evaporation over time. Figure 3b shows an example of participant images at 5, 15, 25, 35, 45 and 55 minutes after painting an image group.

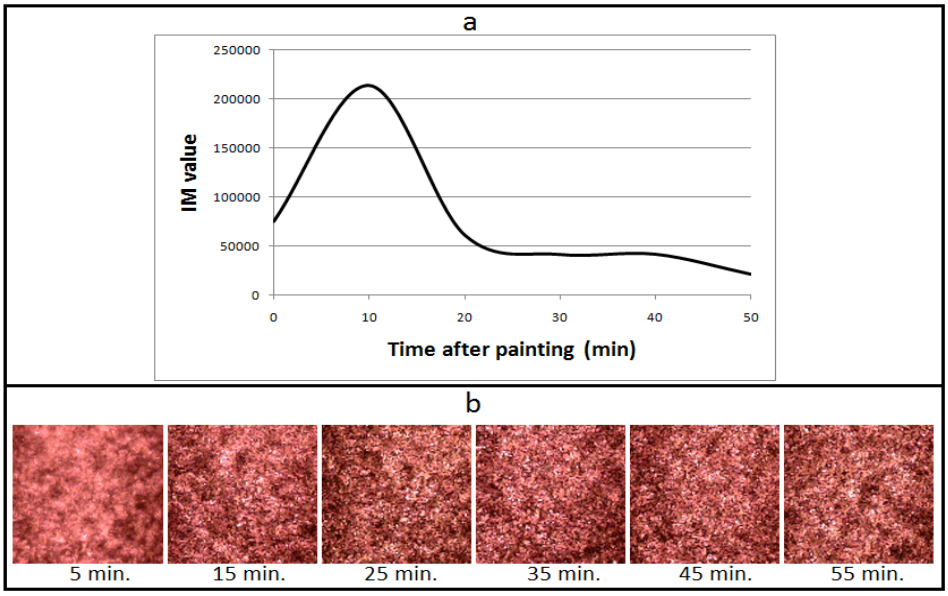

Figure 3 IM values for drying ink on a coin surface (a) and examples of participant images in each collected time

It can be observed that in the first image group the numerical result was inconsistent with expectation. Evaporation activity is expected to be more frenetic a few moments after painting, but IM did not show numerical output in this sense. The hypothesis is that evaporation occurs in higher frequency than rate acquisition, thus the speckle pattern is not completely or even partially formed. In order to confirm this speculation, contrast was calculated according to the methodology. Figure 4 presents the mean contrast for each image group.

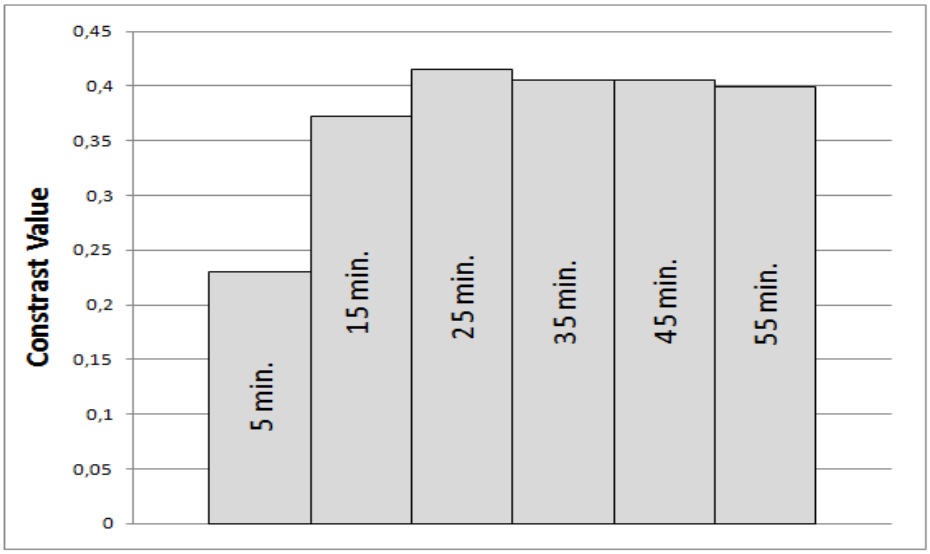

Figure 4 Mean value of contrast for each image group

The contrast value is lower in the first imagery group, indicating a non-formed speckle pattern, and consequently hindering the numerical analysis performed by IM method. The homogeneity is proposed as a complementary pre-analysis in order to give information about the distribution of spatial activity, and the type of main analysis may be chosen. If homogeneity is at low level, graphic analysis is recommended instead of numerical methods unless numerical analysis is performed in the homogeneous area inside the heterogeneous BSL image. Figure 5 shows a classic numerical analysis for fungus (*Aspergillus Flavus*) in tissue culture and for bean seeds. However, fungus growing was not homogeneous and the samples present a high variation coefficient. Figure 5b shows the mean variation coefficient for IM in the sub-areas inside BSL image groups. Similarly, Figure 5c and 5d presents the analysis for bean seeds with a more homogeneous and well-controlled biologic process, following a defined methodology to prepare and illuminate samples (BRAGA et al., 2007).

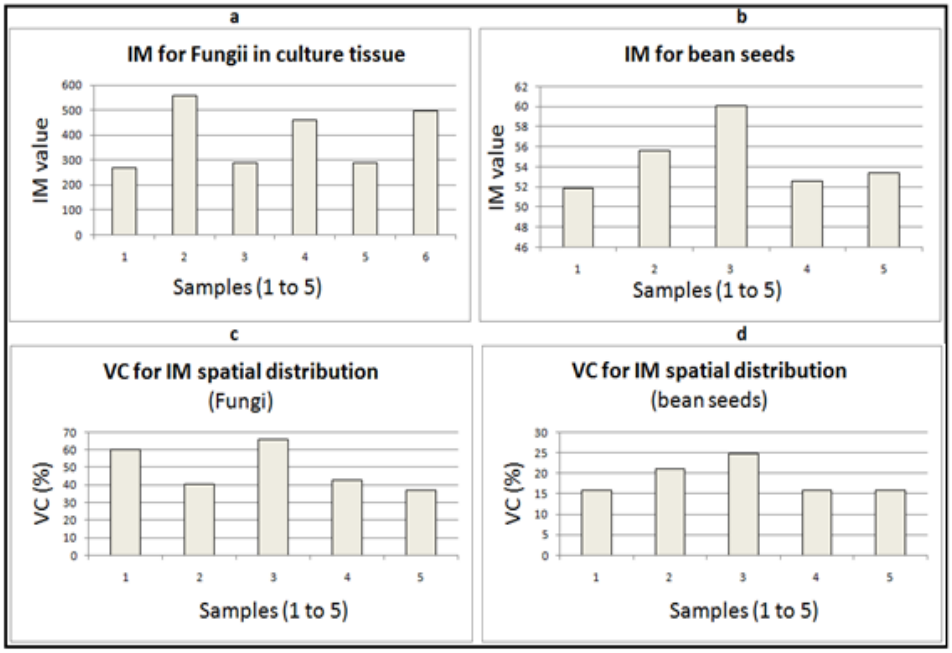

Figure 5 BSL numerical analysis for high dispersion of spatial activity (a, b) and for low dispersion of spatial activity

The samples of fungi presented a variation of the order of 35.76%, showing low repeatability in samples with high dispersion of spatial activity, mean of 49.05% of variation between IM for each subarea in BSL images. For bean seeds, variation between samples was 6.10%, which reflects the distribution of spatial activity, mean of 18.67% in this case. Thus, the relation between coherence and viability in numerical analysis is in inverse proportion with the dispersion of spatial activity in BSL images. Thus, a protocol using the homogeneity of BSL images is established to give information whether the main analysis should be numerical or graphical. However, numerical and graphical output could be associated in homogeneous areas inside heterogeneous BSL images.

Therefore, acquiring information about grain size and studying how it affects the main analysis is another possible procedure for BSL quality

requirements. This pre-analysis has the task to eliminate subjectivism in illumination experiments using mathematical tools for acquiring superior image quality of dynamic speckle laser. This procedure provides a better information extraction for positively affecting numerical or graphical main analysis.

3.2 IM improvements

IM without normalisation, IM with new normalisation and with conventional normalisation were tested in biological and non-biological drying process with the absolute values of difference (AVD) method (DAI PRA; PASSONI; RABAL, 2009). Figure 6 shows numerical results for fruit (banana) drying over 5 days by IM variations. Figure 7 shows the percentage variation coefficient (VC) between the samples over the drying days for IM variations, including AVD and non-normalised IM.

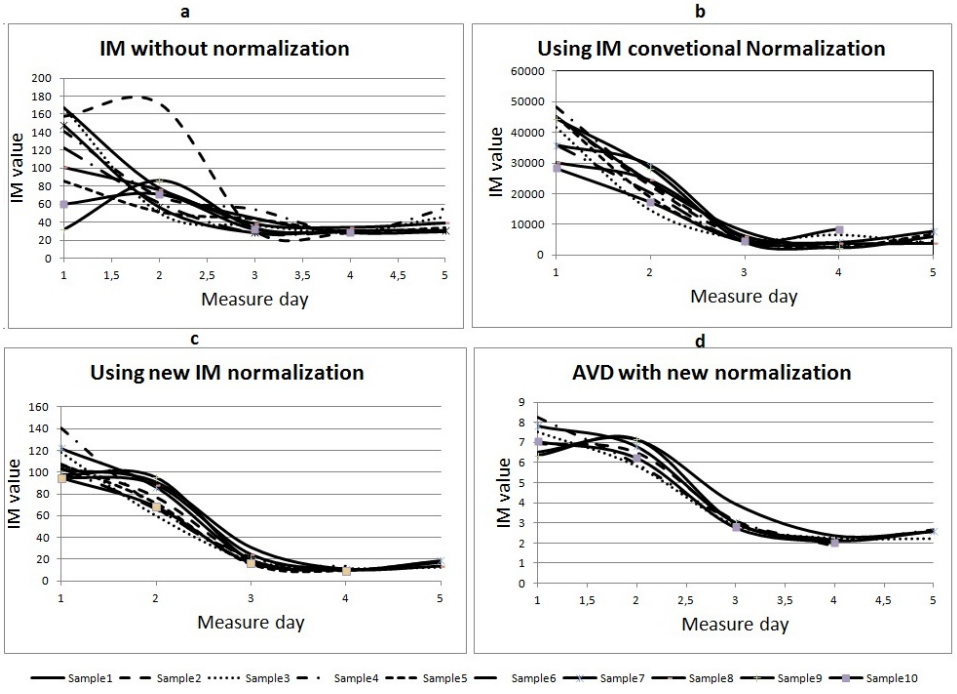

Figure 6 IM variations for measuring activities in drying fruit (a-d)

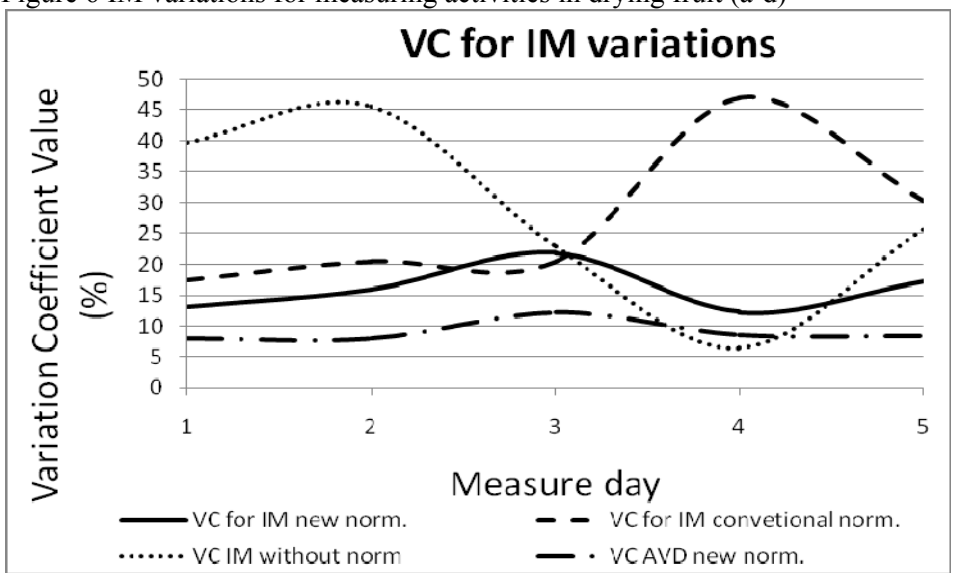

Figure 7 Variation Coefficient (VC) for each measure day

In this case, it can be observed that IM using new normalisation presented lower and stable variation coefficient, especially in low activities. The highest dispersion is observed in IM without normalisation followed by IM with conventional normalisation showing negative high sensitivity. Homogeneity changes with the other normalisations. The ability to maintain repeatability with low dispersion was tested; however, the capacity to differentiate tissue activities has to be tested as well. Similarly, Figure 8 presents a drying process for ink on a coin surface. For non-biological processes the variation coefficient is more stable, although there is still tendency for high dispersion in low activities, as shown in Figure 9.

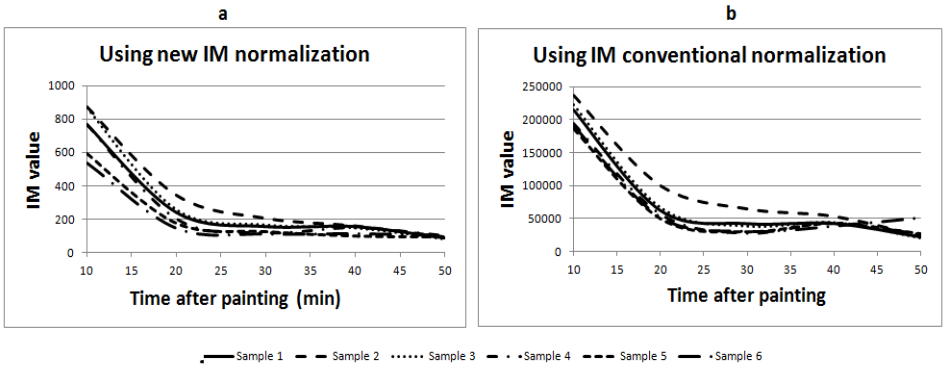

Figure 8 IM test for non-biological drying processes

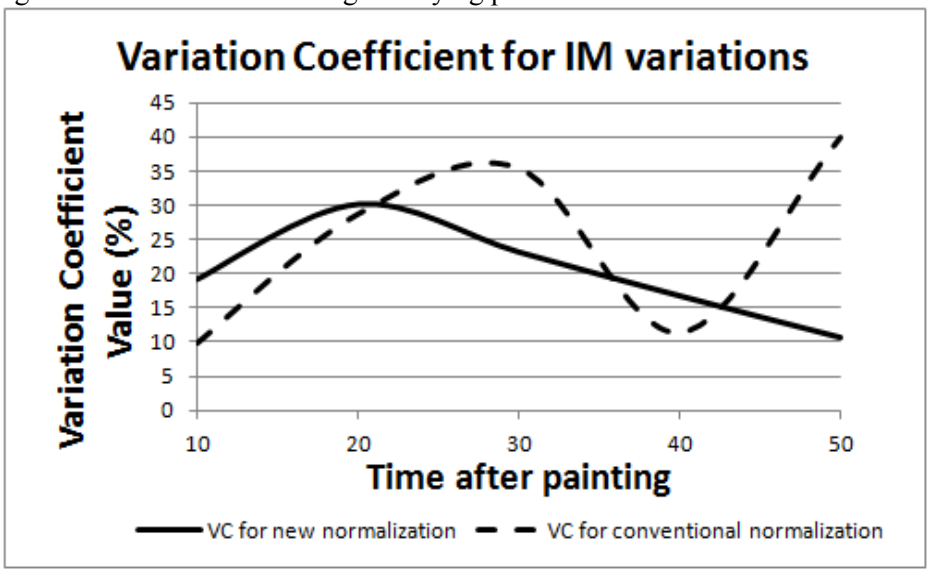

Figure 9 Variation Coefficient (VC) for non biological process

Results for continuous IM are presented in Figure 10. Through video monitoring, the estimated activity shifts moment was 5-5.5 seconds after water contact. This phenomenon occurs abruptly and could represent awakening or germination in the dormancy seed. The different values of window scale were tested, and windows sized 5 and 10 pixel-time were able to determine the phenomena moment with more accuracy. Above 10 in the window scale, the instant of activity increase cannot be estimated with a reasonable precision. The

higher precision estimate for the moment of phenomenon's occurrence was enhanced by using a 5 pixel-time window size (Figure 9c). IM with new (9a) and conventional normalisation (9b) were tested. In order to obtain the activity leap acquired when the seed gain activity, the first derivative was calculated (9d). As it can be observed in Figure 9d, IM with conventional normalisation is more instable with low time information.

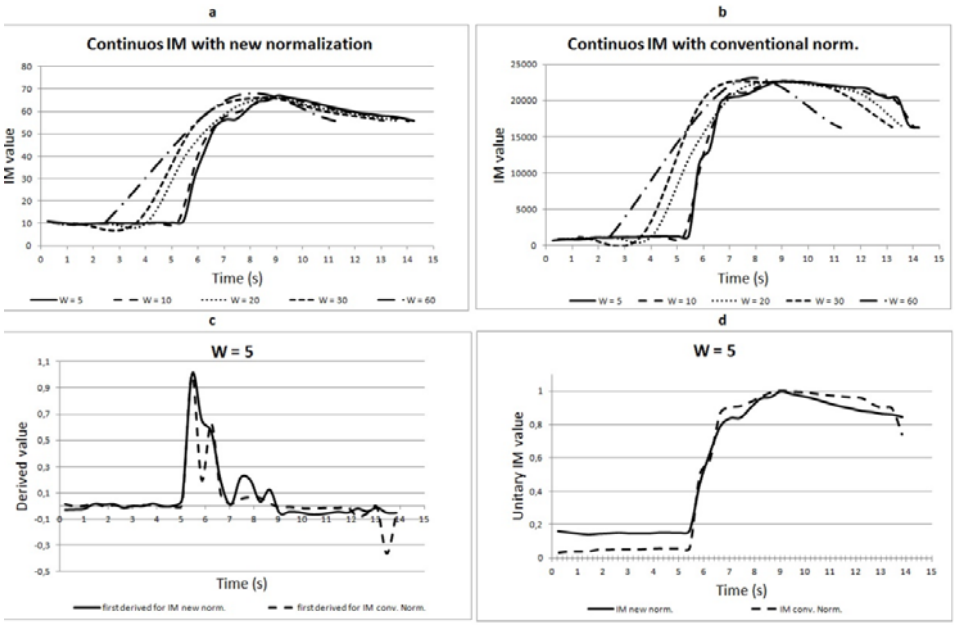

Figure 9 Continuous IM analysis for determining awakening moment in a dormant seed

3.3 Graphical technique

Figure 10 compares Fujii, GD and Standard Deviation (SD) technique for image quality and processing time. As time processing varies with image resolution, number of images and computer performance, the processing time between these methods was put in GD scale of time, as it is the longstanding process. For the images tested, the new technique provided better quality of image than Fujii, and it was significantly faster than GD method. The high

quality of result image in low processing time ensures that SD is a technique suitable for BSL online analysis.

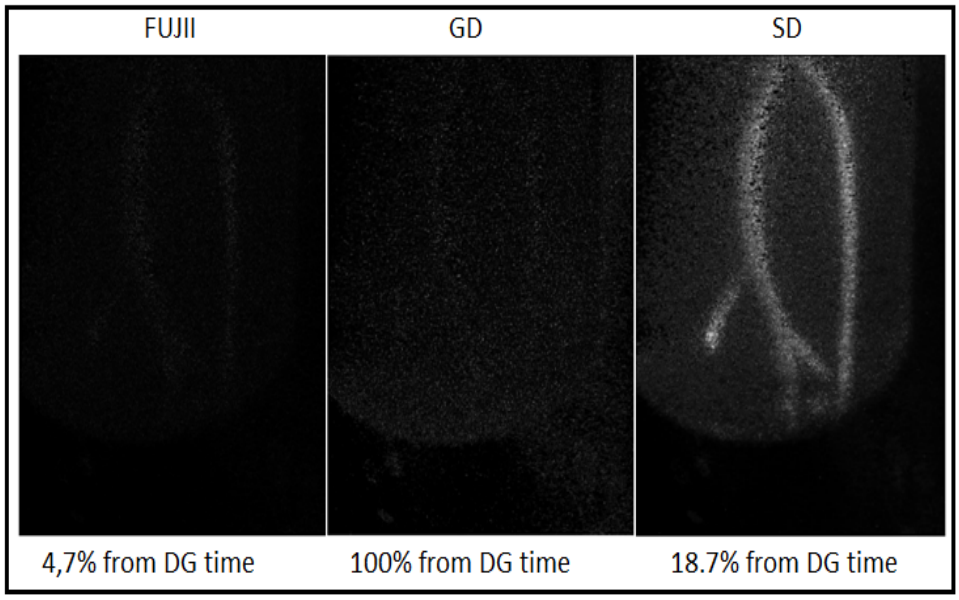

Figure 11 Comparisons between graphical methods

4 CONCLUSION

This study presented an improvement in dynamic speckle laser techniques which opens doors for new analysis processes improving BSL ability to obtain information. It is fundamental to have a proper illumination and experimental setup for acquiring good quality information during the main analysis. The requirements procedure presented here is a step forward to eliminate subjectivism in illumination, in order to enhance reliability in BSL results of the main analysis.

Reduction of high dispersion results in numerical analysis is another achievement. IM high sensitive has a negative effect over some results, thus new normalisation reduces dispersion keeping variation coefficient stable. The new normalisation was performed by making the entire COM equal to one. These accomplishments make BSL a more robust and safer technique, as it keeps low high random variation caused by interaction with light and illuminated object in dynamic speckle phenomena.

SD technique was performed by using dispersion measure for each pixel in time and presented high quality in low processing time, thus it is suitable for online analysis. These new techniques or improvements of conventional methods demonstrated that BSL should be improved in order to be fully employed as optical instrument in several knowledge areas.

REFERENCES

ARIZAGA, R.; CAP, N. L.; RABAL, H. Display of local activity using dynamical speckle patterns**. Optical Engineering**, Bellingham, v. 4, n. 2, p. 287-294, 2002.

ARIZAGA, R.; TRIVI, M.; RABAL, H. J. Speckle time evolution characterization by the co-occurrence matrix analysis. **Optics & Laser Technology**, Benevento, v. 31, p. 163-169, 1999.

BRAGA, R. A. et al. Biological feature isolation by wavelets in biospeckle laser images. **Computers and Electronics in Agriculture**, Amsterdam, v. 58, p. 123-132, 2007.

BRAGA, R. A. et al. Evaluation of activity through dynamic laser speckleusing the absolute value of the differences. **Optics Communications**, Sydney, v. 284, p. 646-650, 2011.

BRAGA, R. A. et al. Live biospeckle laser imaging of root tissues**. European Biophysics Journal**, Berlin, v. 38, n. 5, p. 679-86, 2009.

BRAGA, R. A. et al. Time history speckle pattern under statistical view. **Optics Communications**, Sydney, v. 281, p. 2443-2448, 2008.

BRIERS, J. D. Wavelength dependence of intensity fluctuations in laser speckle patterns from biological specimens. **Optics communications**, Sydney, v. 13, n. 3, p. 324-326, 1975.

CARDOSO, R. R. et al. Frequency signature of water activity by biospeckle laser. **Optics Communications**, Sydney, v. 285, p. 2131-2136, 2011.

CARVALHO, P. H. A. et al. Motility parameters assessment of bovine frozen semen by biospeckle laser (BSL) system. **Biosystems Engineering**, London, v. 102, p. 31-35, 2009.

DAI PRA, A.; PASSONI, I.; RABAL, H. J. Evaluation of laser dynamic speckle signals applying granular computing. **Signal Processing**, Amsterdam, v. 89, n. 3, p. 266-274, 2009.

FUJII, A. H. et al. Blood-flow observed by time-varying laser speckle. **Optics Letters**, Washington, v. 10, n. 3, p. 104-106, 1985.

GONIK, M. M.; MISHIN, A. B.; ZIMNYAKOV, D. Visualization of blood microcirculation parameters in human tissues by time-integrated dynamic speckles analysis. **Annals of the New York Academy of Sciences**, New York, v. 972, p. 325-330, 2002.

HARALICK, R. M.; SHANMUGAN, K.; DINSTEIN, I. Textural Features for Image Classification. **IEEE Trans. Systems, Man and Cybernetic**s, New York, v. 3, n. 6, p.610-621, 1973.

NOBRE, C. M. B. et al. Biospeckle laser spectral analysis under Inertia Moment, Entropy and Cross-Spectrum methods. **Optics Communications**, Sydney, v. 282, n. 11, p. 2236-2242, 2009.

PAJUELO, M. et al. Bio-speckle assessment of bruising in fruits. **Optics and Lasers in Engineering**, Lausanne, v. 40, p. 13-24, 2003.

RABAL, H. J.; BRAGA, R. A. **Dynamic laser speckle and applications**. New York: CRC, 2008.

SKIPETROV, S. E. et al. Noise in laser speckle correlation and imaging techniques. **Optics Express**, Washington, v. 18, n. 14, p. 14519-14534, 2010.

TCHVIALEVA, L. et al. Surface roughness measurement by speckle contrast under the illumination of light with arbitrary spectral profile. **Optics and Lasers in Engineering**, Lausanne, v. 48, n. 7/8, p. 774-778, 2010.

ZDUNEK, A. et al. New nondestructive method based on spatial-temporal speckle correlation technique for evaluation of apples quality during shelf-life. **International Agrophysics**, Lublin, v. 21, p. 305-310, 2007.

APÊNDICE

APÊNDICE A – Transcrição de softwares elaborados

Momento de Inércia:

```
%% MI
% Rafael R. Cardoso
% OBS.: ATUALIZAR S1 E S2!!!

%% Defininções

A                                                                    =
imread('C:\Users\Rafael\Desktop\BMP\Imagens\Fungos\flavus
1\1.bmp'); % Dim. Imagem

B = size(A,2); % n. de colunas
C = size(A,1); % n. e linhas
N = 127; % n. de imagens
K = 10; % Total de pastas, MI no tempo.
s = zeros(1,B);   % s(1,'tamanho da linha a ser usada no MI
')
% Obs.: Se for toda a linha central: s = zeros(1,B).

s1 = C/2; % número da linha em que se deseja calcular o MI
na imagem.
% Obs.: Se for a linha central: s1 = C/2.
s2 = 1; % número da primeira coluna da linha de calculo do
MI.
%Obs.: Se for a linha central da imagem inteira s2=1.

           %(s1,s2)
(s1,s2+size(s,2))
               %%%%%%%%%%%%%%%%%%%%%%%%%%%%%%%%%%%%
                    % Linha do calculo de MI %


X = 2; % 1. MI no tempo;
       % 2. MI para apenas um conjunto;
       % 3. Teste;

%   dir   =   ['C:\Users\Rafael\Desktop\BMP\Imagens\Moeda   -
Márcio\Moeda      Exp.      2      sem      ajuste      de
foco\',num2str(k)','\Image            Sequence            -
Cópia\Altura_Maxima_']; % Para o 1. Diretorio Padrão.
%    dir    =    'C:\Users\Rafael\Desktop\BMP\Imagens\Imagens
nozela\'; % Para X = 2. Diretorio Padrão
```

```
M = zeros(C,B,N);
STS = zeros(size(s,2),N);

MI = zeros(K,1);
AVD = zeros(K,1);
MI_Ari = zeros(K,1);
AVD_Ari = zeros(K,1);
MIIJ = zeros(K,1);



%% MI

if X == 1

            sprintf('Rondando MI')
            m=zeros(1,B,N);

for k=1:K

    sprintf('%d',round(k))

    dir                                                    =
['C:\Users\Rafael\Desktop\BMP\Imagens\Fungos\flavus
',num2str(k)','\'];

for i=1:N
    nome = [dir,num2str(i),'.bmp'];
    matriz= imread(nome,'bmp');
    %matriz = rgb2gray(matriz);
    s(:,:) = matriz(s1:s1,s2:(s2+size(s,2))-1);
    STS(:,i) = s';
    M(:,:,i) = matriz(:,:);
end

sprintf('Comandei as imagens')


%% Salvando o STS

STS = uint8(STS);
imwrite(STS,'sts.bmp')
```

```
sprintf('salvei o sts na pasta de trabalho, dê uma olhada')

% Fim da primeira parte... Agora vamos comandar o MI


im_value = 0;
im_value2 = 0;
im_value3 = 0;
im_value4 = 0;
im_value5 = 0;

%% Criação da Matriz de Ocorrência

%ocm = zeros(256,256);
 % for a=1:B
 %   for b=1:N-1
 %     x=STS(a,b);
 %     y=STS(a,b+1);
 %        if x==0,x=1;
 %        end
 %       if y==0,y=1;
 %     end

  %ocm(x,y) = ocm(x,y) +1;
   %  end
  % end

ocm = graycomatrix(STS,'NumLevels',256);

%% MI

%% O MI foi calculado pela fórmula: MI=(N_ij/(?N_ij )) (i-
j)^2 , em que
%% N_ij é o valor na posição de i,j da MOC

sprintf('Calculando o MI...')


  for x=1:256
    for y=1:256


     im_value  =  ((ocm(x,y))/(sum(sum(ocm))))*((x-y)^2)  +
im_value;
     MI(k,1) = im_value;
```

```
     im_value2  =  ((ocm(x,y))/(sum(sum(ocm))))*(abs(x-y))  +
im_value2;
     AVD(k,1) = im_value2;


     norm = sum(ocm(x,:));
     if norm == 0;
         norm =1;
     end

     im_value3 = (ocm(x,y)*((x-y)^2))/(norm) + im_value3;
     MI_Ari(k,1) = im_value3;

     im_value4 = (ocm(x,y)*(abs(x-y)))/(norm) + im_value4;
     AVD_Ari(k,1) = im_value4;

     im_value5 = (ocm(x,y)*((x-y)^2))/(256) + im_value5;
     MIIJ(k,1) = im_value5;

    end
  end

  Str = [im_value];
   sprintf('%f', Str)

end
end

%%%%%%%%%%%%%%%%%%%%%%%%%%%%%%%%%%%%%%%%%%%%%%%%%%%%%%%%%%%%%%%%%%%%%%%%%%%%
%%%%%%%%%%%%%%%%
%% 2

if X == 2

        sprintf('Rodando MI')
        m=zeros(1,B,N);

    for i=1:N
        nome = [dir,num2str(i),'.bmp'];
        matriz= imread(nome,'bmp');
        matriz = rgb2gray(matriz);
        s(:,:) = matriz(s1:s1,s2:(s2+size(s,2))-1);
        STS(:,i) = s';
        %M(:,:,i) = matriz(:,:);
    end
```

```
sprintf('Comandei as imagens')

%% Salvando o STS

STS = uint8(STS);
imwrite(STS,'sts.bmp')

sprintf('salvei o sts na pasta de trabalho, dê uma olhada')

% Fim da primeira parte... Agora vamos comandar o MI

im_value = 0; im_value2 = 0;
im_value3 = 0; im_value4 = 0;
im_value5 = 0;

%% Criação da Matriz de Ocorrência

ocm = zeros(256,256);
  for a=1:size(STS,1)
    for b=1:N-1
      x=STS(a,b);
      y=STS(a,b+1);
         if x==0,x=1;
         end
        if y==0,y=1;
      end

  ocm(x,y) = ocm(x,y) +1;
     end
   end

%ocm = graycomatrix(STS,'NumLevels',256);

%% MI

%% O MI foi calculado pela fórmula: MI=(N_ij/(?N_ij )) (i-
j)^2 , em que
%% N_ij é o valor na posição de i,j da MOC

sprintf('Calculando o MI...')


    for x=1:256
        for y=1:256
```

```
            im_value   =   ((ocm(x,y))/(sum(sum(ocm))))*((x-
y)^2) + im_value;
            MI = im_value;

            im_value2                                        =
((ocm(x,y))/(sum(sum(ocm))))*(abs(x-y)) + im_value2;
            AVD = im_value2;


            norm = sum(ocm(x,:));
            if norm == 0;
               norm =1;
            end

            im_value3   =   (ocm(x,y)*((x-y)^2))/(norm)   +
im_value3;
            MI_Ari = im_value3;

            im_value4   =   (ocm(x,y)*(abs(x-y)))/(norm)   +
im_value4;
            AVD_Ari = im_value4;

            im_value5   =   (ocm(x,y)*((x-y)^2))/(256)   +
im_value5;
            MIIJ = im_value5;

        end
    end

  Str = [im_value];
   sprintf('%f', Str)
end



%%%%%%%%%%%%%%%%%%%%%%%%%%%%%%%%%%%%%%%%%%%%%%%%%%%%%%%%%%%%%%%%%%%%%%%
%%%%%%%%%%%%%%%

if X == 3


            sprintf('Rondando MI com pré-processamento')
```

```
for k=1:K

    sprintf('%d',round(k))

    dir   =  ['L:\Juliana\',num2str(k)','_dia\Banana\Amostra
2\banana2_']; % Diretório

for i=1:N
    nome = [dir,num2str(i),'.bmp'];
    matriz= rangefilt(imread(nome,'bmp'));
    s(:,:) = matriz(C/2:C/2,1:B);
    STS(:,i) = s';
end

sprintf('Comandei as imagens')


%% Salvando o STS

STS = uint8(STS);
imwrite(STS,'sts.bmp')

sprintf('salvei o sts na pasta de trabalho, dê uma olhada')

% Fim da primeira parte... Agora vamos comandar o MI


im_value = 0;
im_value2 = 0;
im_value3 = 0;
im_value4 = 0;
%% Criação da Matriz de Ocorrência

ocm = zeros(256,256);
  for a=1:size(STS,1)
    for b=1:N-1
      x=STS(a,b);
      y=STS(a,b+1);
         if x==0,x=1;
         end
        if y==0,y=1;
```

```
      end

  ocm(x,y) = ocm(x,y) +1;
     end
   end

%ocm = graycomatrix(STS,'NumLevels',256);

%% MI

%% O MI foi calculado pela fórmula: MI=(N_ij/(?N_ij )) (i-
j)^2 , em que
%% N_ij é o valor na posição de i,j da MOC

sprintf('Calculando o MI...')

%somatorio = 0;
%for x=1:256
 %   for y=1:256
%somatorio = ocm(x,y) + somatorio;

 %   end
%end


  for x=1:256
    for y=1:256


     im_value  =  ((ocm(x,y))/(sum(sum(ocm))))*((x-y)^2)  +
im_value;
     MI(k,1) = im_value;

     im_value2  =  ((ocm(x,y))/(sum(sum(ocm))))*(abs(x-y))  +
im_value2;
     AVD(k,1) = im_value2;


     norm = sum(ocm(x,:));
     if norm == 0;
         norm =1;
     end

     im_value3 = (ocm(x,y)*((x-y)^2))/(norm) + im_value3;
     MIb(k,1) = im_value3;
```

```
     im_value4 = (ocm(x,y)*(abs(x-y)))/(norm) + im_value;
     AVDb(k,1) = im_value4;




    end
  end

  Str = [im_value];
   sprintf('%f', Str)

end
end
```

Requisitos para qualidade de imagem do BSL:

```
%% Homogeneidade
% Rafael R. Cardoso



%% Definições

A   =   imread('C:\Users\Rafael\Desktop\BMP\Imagens\Imagens
improvements\Milho\milho1.bmp'); % Diretorio de uma Img. do
conjunto.

B = size(A,2); % n. de colunas
C = size(A,1); % n. e linhas

dir     =     'C:\Users\Rafael\Desktop\BMP\Imagens\Imagens
improvements\Milho\milho'; % Diretorio padrão.
N = 64; % n. de imagens
t= 40; % Tamanho das sub.áreas

n = ((C/t)*(B/t)); % n. de sub.áreas.

m1 = zeros(1,t,N); % Sub.área do MI;
m2 = zeros(t,t,N); % Sub.área do Contraste;

im_value = 0;
```

```
im_value2 = 0;

MI = zeros(fix(C/t),fix(B/t));
AVD = zeros(fix(C/t),fix(B/t));
MI_R = zeros(fix(C/t),fix(B/t));
AVD_R = zeros(fix(C/t),fix(B/t));
Cc = zeros(fix(C/t),fix(B/t));
Sat = zeros(fix(C/t),fix(B/t));
Dark = zeros(fix(C/t),fix(B/t));
ocm2 = zeros(256,256,N);


       nsat1 = zeros(fix(C/t),fix(B/t));
       ndark1 = zeros(fix(C/t),fix(B/t));
       nnormal1 = zeros(fix(C/t),fix(B/t));
%% Testando área t


%% Abrindo sub.áreas

for X1 =1:t:C-t

    sprintf('%d',round(X1))

    ocm = zeros(256,256);

        for Y1 = 1:t:B+1-t



                  for i=1:N
                      nome = [dir,num2str(i),'.bmp'];
                      matriz= imread(nome,'bmp');
                      %matriz = rgb2gray(matriz);
                      m1(:,:,i)    =    matriz(X1-1+t/2:X1-
1+t/2,Y1:Y1+t-1);
                      m2(:,:,i)      =      matriz(X1:X1+t-
1,Y1:Y1+t-1);
                  end



%% Calculando MI

R = zeros(t,N);
```

```
R = reshape(m1,[t N]);

STS = zeros(t,N);
STS(:,:) = R(1:t,1:N);

%% Salvando o STS

STS = uint8(STS);
imwrite(STS,'sts.bmp')

%sprintf('salvei  o  sts  na  pasta  de  trabalho,  dê  uma
olhada')

% Fim da primeira parte... Agora vamos comandar o MI

im_value = 0;
im_value2 = 0;
im_value3 = 0;
im_value4 = 0;
%% Criação da Matriz de Ocorrência


  %for a=1:t
   % for b=1:N-1
     % x=STS(a,b);
     % y=STS(a,b+1);
      %   if x==0,x=1;
     %    end
    %    if y==0,y=1;
   %     end
  %
  % ocm(x,y) = ocm(x,y) +1;
 %    end
%   end

ocm = graycomatrix(STS,'NumLevels',256);
%% MI

  for x=1:256
    for y=1:256


     im_value  =  ((ocm(x,y)/(sum(sum(ocm)))))*((x-y)^2)  +
im_value;
     MI((X1+t-1)/t,(Y1+t-1)/t)    =    im_value;    %    MI
normalização cardoso
```

```
     im_value2  =  ((ocm(x,y)/(sum(sum(ocm)))))*(abs(x-y))  +
im_value2;
     AVD((X1+t-1)/t,(Y1+t-1)/t)    =    im_value2;    %    AVD
normalização cardoso


     norm = sum(ocm(x,:));
     if norm == 0
         norm = 1;
     end

     im_value3 = ((ocm(x,y))/(norm))*((x-y)^2) + im_value3;
     MI_R((X1+t-1)/t,(Y1+t-1)/t) = im_value3;

     im_value4     =     ((ocm(x,y))/(norm))*(abs(x-y))     +
im_value4;
     AVD_R((X1+t-1)/t,(Y1+t-1)/t) = im_value4;


    end
  end

 % Str = [im_value];
  % sprintf('%f', Str)


        %% Calculando Contraste, áreas saturadas e escuras

        Cc((X1+t-1)/t,(Y1+t-1)/t) = std2(m2)/mean2(m2);
        ocm2 = zeros(256,256,N);


       sat = m2>=255;
       dark = m2<=1;
       normal = m2>1 & m2<255;

       nsat1((X1+t-1)/t,(Y1+t-1)/t) = sum(sum(sum(sat)));
       ndark1((X1+t-1)/t,(Y1+t-1)/t) = sum(sum(sum(dark)));
       nnormal1((X1+t-1)/t,(Y1+t-1)/t)                    =
sum(sum(sum(normal)));

       nsat = sum(sum(sum(sat)));
       ndark = sum(sum(sum(dark)));
       nnormal = sum(sum(sum(normal)));
```

```
        %% Definição de áreas saturadas e escuras


        if nsat >= (t^2)*N*0.05

           r1 = 255;

        end

       if ndark >= (t^2)*N*0.05

          r2 = 0;

       end

       if nnormal > (t^2)*N*0.95

          r1 = 128;
          r2 = 128;

       end

       Sat((X1+t-1)/t,(Y1+t-1)/t) = r1;
       Dark((X1+t-1)/t,(Y1+t-1)/t) = r2;

         end

end


%%

sprintf('homogeneidade:')
invCV2 = 1- (std2(AVD)/mean2(AVD));
invCV = 1- (std2(MI)/mean2(MI))^-1;
sprintf('%f',invCV2)


mi2 = AVD/(max(max(AVD)));
mi = MI/(max(max(MI)));
CCm = mean2(Cc);

%% Plotando Resultados
figure(1)
```

```
colormap(gray)
ax(1) = subplot(1,2,1);
imagesc(Sat); title('Saturação')
% grid
axis image
xlabel('Área Saturada - Branco')
ylabel('Área Escura - Normal')
ax(2) = subplot(1,2,2);
imagesc(Sat); title('Áreas Escuras')
% grid
axis image
xlabel('Área Escura - Preto')
ylabel('Área Normal - Branco')



figure(2)
colormap(gray)
ax(1) = subplot(1,2,1);
imshow(Cc); title('Contraste')
colorbar
%grid on
axis image
xlabel(sprintf('Contraste Me: %f.',CCm))
ax(2) = subplot(122);
image(mi*255);title('MI')
%grid on
axis image
colorbar
xlabel(sprintf('Homogendeidade: %f.',invCV))
```

MI contínuo:

```
%% MI "continuo"
% Rafael R. Cardoso
% 15/04/2011

%% Defininções

A                                                          =
imread('C:\Users\Rafael\Desktop\BMP\Imagens\Semente\1.bmp')
; % Dim. Imagem

B = size(A,2); % n. de colunas
C = size(A,1); % n. e linhas
N = 180; % n. de imagens
```

```
J = 5; % Janela do MI continuo. (use o q vc quer + 1)

X = 1;  % 1. N.MI = N-J;
        % 2. N.MI = N/J;


s = zeros(1,45);    % s(1,'tamanho da linha a ser usada no
MI ')
% Obs.: Se for toda a linha central: s = zeros(1,B).

s1 = 265; % número da linha em que se deseja calcular o MI
na imagem.
% Obs.: Se for a linha central: s1 = C/2.
s2 = 185; % número da primeira coluna da linha de calculo
do MI.
%Obs.: Se for a linha central da imagem inteira s2=1.

           %(s1,s2)
(s1,s2+size(s,2))
              %%%%%%%%%%%%%%%%%%%%%%%%%%%%%%%%%%%%
                   % Linha do calculo de MI %


dir   =  'C:\Users\Rafael\Desktop\BMP\Imagens\Semente\';  %
Diretorio Padrão



%%%%%%%%%%%%%%%%%%%%%%%%%%%%%%%%%%%%%%%%%%%%%%%%%%%%%%%%%%%
%%%%%%%%%%%%%%%%
%M = zeros(C,B,N);
STS = zeros(size(s,2),N);
MI = zeros((N),1); % MI normalização Cardoso;
AVD = zeros((N),1); % AVD normalização Cardoso;
MI_Ari = zeros((N),1); % MI normalização Arizaga et al.
(1999);
AVD_Ari = zeros((N),1); % AVD normalização Arizaga et al.
(1999).
MIIJ = zeros((N),1);

%% Janela tipo 1

if X == 1
%% MI
```

```
    for i=1:J:N
        nome = [dir,num2str(i),'.bmp'];
        matriz= imread(nome,'bmp');
        s(:,:) = matriz(s1:s1,s2:(s2+size(s,2))-1);
        STS(:,i) = s';
        %M(:,:,i) = matriz(:,:);
    end



%% Salvando o STS

STS = uint8(STS);
imwrite(STS,'sts.bmp')



% Fim da primeira parte... Agora vamos comandar o MI

im_value = 0; im_value2 = 0;
im_value3 = 0; im_value4 = 0;
im_value5 = 0;

%% Criação da Matriz de Ocorrência

for b1=J+1:J:N

sprintf('%f',(100*b1/N))


ocm = zeros(256,256);
  for a=1:size(STS,1)
    for b=b1-J:b1
      x=STS(a,b);
      y=STS(a,b+1);
         if x==0,x=1;
         end
        if y==0,y=1;
      end

  ocm(x,y) = ocm(x,y) +1;
     end
   end
```

```
%ocm = graycomatrix(STS,'NumLevels',256);

%% MI

%% O MI foi calculado pela fórmula: MI=(N_ij/(?N_ij )) (i-
j)^2 , em que
%% N_ij é o valor na posição de i,j da MOC



    for x=1:256
        for y=1:256


            im_value   =   ((ocm(x,y))/(sum(sum(ocm))))*((x-
y)^2) + im_value;
            MI((b1-1)/J,1) = im_value;

            im_value2                                       =
((ocm(x,y))/(sum(sum(ocm))))*(abs(x-y)) + im_value2;
            AVD((b1-1)/J,1) = im_value2;


            norm = sum(ocm(x,:));
            if norm == 0;
               norm =1;
            end

            im_value3   =   (ocm(x,y)*((x-y)^2))/(norm)   +
im_value3;
            MI_Ari((b1-1)/J,1) = im_value3;

            im_value4   =   (ocm(x,y)*(abs(x-y)))/(norm)   +
im_value4;
            AVD_Ari((b1-1)/J,1) = im_value4;

            im_value5    =    (ocm(x,y)*((x-y)^2))/(256)    +
im_value5;
            MIIJ((b1-1)/J,1) = im_value5;

        end
    end
end
```

```
  Str = [im_value];

end

%%%%%%%%%%%%%%%%%%%%%%%%%%%%%%%%%%%%%%%%%%%%%%%%%%%%%%%%%%%
%%%%%%%%%%%%%%%%

%% Janela tipo 2

if X == 2


    %% MI


    STS = zeros(size(s,2),J);

    for k =J:J:N


        sprintf('%f',(100*k/N))
       for i = (k-(J-1)):k


        nome = [dir,num2str(i),'.bmp'];
        matriz= imread(nome,'bmp');
        s(:,:) = matriz(s1:s1,s2:(s2+size(s,2))-1);
        STS(:,i) = s';
        %M(:,:,i) = matriz(:,:);
       end



%% Salvando o STS

STS = uint8(STS);
imwrite(STS,'sts.bmp')



% Fim da primeira parte... Agora vamos comandar o MI

im_value = 0; im_value2 = 0;
im_value3 = 0; im_value4 = 0;
im_value5 = 0;
```

```
%% Criação da Matriz de Ocorrência

ocm = zeros(256,256);
  for a=1:size(STS,1)
    for b=1:size(STS,2)-1
      x=STS(a,b);
      y=STS(a,b+1);
         if x==0,x=1;
         end
        if y==0,y=1;
      end

  ocm(x,y) = ocm(x,y) +1;
     end
   end

%ocm = graycomatrix(STS,'NumLevels',256);

%% MI

%% O MI foi calculado pela fórmula: MI=(N_ij/(?N_ij )) (i-
j)^2 , em que
%% N_ij é o valor na posição de i,j da MOC




    for x=1:256
        for y=1:256


            im_value   =   ((ocm(x,y))/(sum(sum(ocm))))*((x-
y)^2) + im_value;
            MI(k/J,1) = im_value;

            im_value2                                      =
((ocm(x,y))/(sum(sum(ocm))))*(abs(x-y)) + im_value2;
            AVD(k/J,1) = im_value2;


            norm = sum(ocm(x,:));
            if norm == 0;
               norm =1;
            end
```

```
            im_value3    =    (ocm(x,y)*((x-y)^2))/(norm)    +
im_value3;
            MI_Ari(k/J,1) = im_value3;

            im_value4   =   (ocm(x,y)*(abs(x-y)))/(norm)   +
im_value4;
            AVD_Ari(k/J,1) = im_value4;

            im_value5    =    (ocm(x,y)*((x-y)^2))/(256)    +
im_value5;
            MIIJ(k/J,1) = im_value5;

        end
    end
    end
  Str = [im_value];
end
```

Programa gráfico:

```
        %% Cabeçalho
%%%%%%%%%%%%%%%%%%%%%%%%         DG,Fujii         e         SD
%%%%%%%%%%%%%%%%%%%%%%%%%%%%%%%%%%%%
%%%%%%%%%%%%%%%%%%%%%%%%%%%%%%%%%%%%%%%%%%%%%%%%%%%%%%%%%%%%
%%%%%%%%%%%%%%%%
%%%%%%%%%%%%%%%%%%%%%         Rafael         R.         Cardoso,
%%%%%%%%%%%%%%%%%%%%%%%%%%%%%%%%%%
%%%%%%%%%%%%%%%%%%%%%%%%%%%%%%%%%%%%%%%%%%%%%%%%%%%%%%%%%%%%
%%%%%%%%%%%%%%%%
        %% Definições


N = 100; % número de imagens

Nome1    =    ('C:\Users\Rafael\Desktop\BMP\Imagens\Milho    -
Cópia\milho1.bmp'); % Nome da Imagem 1 + diretório;
NomeP    =    ('C:\Users\Rafael\Desktop\BMP\Imagens\Milho    -
Cópia\milho'); % Nome padrão das Imgagens + diretório;

NomeR  =  'milho_SD';  %  Nome  da  imagem  resultado  que  será
salva.

X = 3;  % 1 = DG
```

```
        % 2 = Fujii
        % 3 = SD

        %% Abrindo as imagens


A = imread(Nome1);

B = size(A,2); % n. de colunas
C = size(A,1); % n. e linhas

Imagem = zeros(C,(B-1));
Imagem(:,:) = A(1:C,1:B-1);
Imagem = uint8(Imagem);

m=zeros(C,B,N);


for i=1:N
    nome = [NomeP,num2str(i),'.bmp'];
    matriz= imread(nome,'bmp');
    m(:,:,i) = matriz(1:C,1:B);
end




        %% Calculando DG (X=0)




if X == 1

     sprintf('Calculando DG...')

DG= zeros(C,B);
dg = zeros(C,B);

for k=1:N-1
    for j=1:N-k

    dg(:,:) = (abs(m(:,:,k+j) - m(:,:,k))); %(m(x,y,i+1) +
m(x,y,i)))+Fuji);
    DG(:,:) = dg(:,:) + DG(:,:);
```

```
    end
end


DG = (DG/max(max(DG)));
imshow(DG);
title('DG');
saveas(gcf,NomeR,'jpg');


end


%% Calculando Fujii



if X == 2

    sprintf('Calculando Fujii...')

Fujii = zeros(C,B);
Fj = zeros(C,B);

 for k=1:N-1


    Fj(:,:) = (abs((m(:,:,k) - m(:,:,k+1)))./((m(:,:,k) +
m(:,:,k+1)));
    Fujii(:,:) = Fj(:,:) + Fujii(:,:);


 end



Fujii = (Fujii/max(max(Fujii)));
imshow(Fujii);
title('Fujii');
saveas(gcf,NomeR,'jpg');

end
```

```
%% Teste

if X == 3

    sprintf('Calculando Parametro...')

SD = zeros(C,B);

    for x=1:C
       for y=1:B

    SD(x,y) = abs(std2(m(x,y,:)));%/mean2(m(x,y,:)));

       end
    end




SD = SD/(max(max(SD)));

imshow(SD);
title('SD');
imwrite(SD,'DP_original','bmp');
saveas(gcf,NomeR,'jpg');

end

%%%%FIM!
% Comandei!


 sprintf('Salvei a imagem na pasta de trabalho')
```

Programa gráfico em freq.:

```
        %% Cabeçalho
%%%%%%%%%%%%%%%%%%%%%%%%      DG,Fujii      e      CV      em
Freq.%%%%%%%%%%%%%%%%%%%%%%%%%%%%
%%%%%%%%%%%%%%%%%%%%%%%%%%%%%%%%%%%%%%%%%%%%%%%%%%%%%%%%%%%%
%%%%%%%%%%%%%%%%
%%%%%%%%%%%%%%%%%%%%%%%%%%      Rafael      R.      Cardoso
%%%%%%%%%%%%%%%%%%%%%%%%%%%%%
```

```
        %% Definições


N = 64; % número de imagens

Nome1    =    ('D:\Rafael    -    Ufla\Imagens    -    Trabalho
Ufla\milho\kato\Results\Reconstruindo    apenas    a    faixa
1\1.bmp'); % Nome da Imagem 1 + diretório;
NomeP    =    ('D:\Rafael    -    Ufla\Imagens    -    Trabalho
Ufla\milho\kato\Results\Reconstruindo apenas a faixa '); %
Nome padrão das Imgagens + diretório;
result=    ('C:\Users\Rafael\Desktop\IMPROVEMENTS\Milho    em
escalas de freq\DG'); % Nome do Dir. Resultados.

K = 21; % N. Faixas de Freq.

X = 1;  % 1 = DG
        % 2 = Fujii
        % 3 = SD

        %% Abrindo as imagens


A = imread(Nome1);

B = size(A,2); % n. de colunas
C = size(A,1); % n. e linhas

m=zeros(C,B,N);

        %% Calculando DG (X=0)


if X == 1

    for k=1:K

        sprintf('%d',round(k))

        dir = [NomeP,num2str(k),'\'];

        sprintf('Calculando DG...')

        for i=1:N
```

```
            nome = [dir,num2str(i),'.bmp'];
            matriz= imread(nome,'bmp');
            m(:,:,i) = matriz(:,:);
        end

DG= zeros(C,B);
dg = zeros(C,B);

for n=1:N-1
    for n1=1:N-n

    dg(:,:) = (abs(m(:,:,n+n1) - m(:,:,n)));
    DG(:,:) = dg(:,:) + DG(:,:);

    end
end




            DG = (DG/max(max(DG)));

            nome2 = [result,num2str(k),'.bmp'];

            imwrite(DG,nome2,'bmp');

    end
end


%% Calculando Fujii



if X == 2

   for k=1:K

        sprintf('%d',round(k))

        dir = [NomeP,num2str(k),'\'];

        sprintf('Calculando Fujii...')

        for i=1:N
```

```
            nome = [dir,num2str(i),'.bmp'];
            matriz= imread(nome,'bmp');
            m(:,:,i) = matriz(:,:);
        end

Fujii = zeros(C,B);
Fj = zeros(C,B);



 for n=1:N-1


    Fj(:,:) = (abs((m(:,:,n) - m(:,:,n+1)))./(1+((m(:,:,n)
+ m(:,:,n+1))));
    Fujii(:,:) = Fj(:,:) + Fujii(:,:);


 end


        Fujii = (Fujii/(max(max(Fujii))));

        %Fujii = uint8(Fujii);

        %Fujii = imadjust(Fujii);

        nome2 = [result,num2str(k),'.bmp'];

        imwrite(Fujii,nome2,'bmp');

   end
end


%% Teste

if X == 3

    for k=1:K

        CV = zeros(C,B);

        sprintf('%d',round(k))
```

```
        sprintf('Calculando SD...')

        dir = [NomeP,num2str(k),'\'];

        for i=1:N
            nome = [dir,num2str(i),'.bmp'];
            matriz= imread(nome,'bmp');
            m(:,:,i) = matriz(:,:);

        end

SD = zeros(C,B);

    for x=1:C
       for y=1:B

    SD(x,y) = abs(std2(m(x,y,:)));%/mean2(m(x,y,:)));

       end
    end


        SD = SD/(max(max(SD)));

        nome2 = [result,num2str(k),'.bmp'];

        imwrite(SD,nome2,'bmp');

    end
end

%%%%FIM!
% Comandei!
```